Extreme Environment Video Diagnostic for a Lithium Lorentz Force Accelerator

Joshua Umansky-Castro, '17

Submitted to the
Department of Mechanical and Aerospace Engineering
Princeton University
in partial fulfillment of the requirements of
Undergraduate Independent Work.

Final Report

May 3, 2017

Edgar Choueiri
N. Jeremy Kasdin
MAE 442
65 pages
File Copy

This thesis represents my own work in accordance with University regulations.

Abstract

The design is presented of a video diagnostic system that was developed for the lithium Lorentz Force Accelerator. Obtaining head on footage of the thruster, the system provides visual confirmation of propellant mass distribution, and supports the study of the onset phenomenon through correlation with voltage oscillations. The system can operate for over 3 days under vacuum off battery power alone, and features several layers of protection to withstand the extreme environment, including a transparent film scrolling mechanism that will maintain visual in spite of condensing lithium. Manufactured and tested, successful operation of the video diagnostic system has been confirmed.

Acknowledgements

There are a number of people who Id like to thank for supporting me throughout this past year as I have completed my senior thesis:

Firstly, I must express my extreme gratitude to Will Coogan, for his daily support on this project. Will had always been there to answer my questions, offer suggestions and brainstorm designs, in spite of all other commitments and responsibilities. Most importantly, he taught me the machining skills necessary to bring this project to life, and leave Princeton with the engineering background necessary to pursue future projects. I would also like to thank the other members of the EPPDyL, Matthew Feldman, Jack Hollingsworth Sebastin Rojas Mata, Pierre-Yves Taunay, Christopher Wordingham, for both their guidance and good company throughout my time in the lab.

Outside of the EP lab, I would like to thank several members of the MAE staff, who provided advice and suggestions that were indispensable to the success of the project. Jon Prevost, who offered suggestions for initial design concepts, provided guidance on charging circuit design, and helped identify a battery that would enable the system to function successfully. Through my course on microprocessors, Jon had also worked tirelessly to aid us in our project, providing me with the electronics background necessary to not only complete this thesis, but tackle future challenges on projects in industry and elsewhere. I would also like to express my thanks to Glenn Northey and Al Gaillard, for showing me how to design and build, introducing me to many of the manufacturing techniques necessary to complete this project. They provided me with the skills necessary to self-identify as an engineer, guiding me through my design courses, and always being available to answer questions and offer suggestions on this thesis.

Within the MAE faculty and administration, I would like to thank Professor Jeremy Kasdin and Professor Rob Stengel, for inspiring me to pursue aerospace. Through courses in orbital mechanics and space systems design, they have provided me with a strong background for future work in the field of space exploration. Most importantly, I would like to express my gratitude to Jo Ann Kropilak-Love, for being a constant source of support throughout the year. From providing logistical help to just being someone to have a fun chat with, Jo Ann had always taken time out of her extremely busy days to be there for me, and all of the students within the MAE department.

Both in and out of the E-Quad, I would like to thank my fellow students for be-

ing a source of joy and support throughout this project and my overall journey at Princeton. My roommates, John and Ujjwal, for their emotional support and good company throughout all of the struggles Ive faced. My fellow EWBers, including Corrie, Susannah, Jiayang, Amanda and Kasturi, for the friendship developed through countless hours together both on campus and in the highlands of Peru, as we worked together to improve lives through what became my first real engineering experience. The members of Brown Co-op, including Mariana, AJ, Lulu, Dominique, Zoe, David, Grace, Justin and Travis, for their companionship and delicious food at my home away from lab, especially Susannah, who always brightened my day through our Equad lunch breaks and dinner cookshifts. Most importantly, I would like to thank the MAE Wilcox crew, for the friendship that got me through the countless nights of problems sets, the hours spent debugging in lab, and the chaos of our design projects. Because of them, these past few years have been such an enjoyable journey, and I am proud to graduate among such an amazing group of future engineers.

Last but not least, I would like to thank my parents and my sisters Hannah and Rachel, for being there for me in all that I do. For all of the sacrifices that brought me here, and for the constant support and love that motivated me throughout. Thank you.

To my parents, for always believing in me.

Contents

List of Symbols

Chapter 1

Introduction

1.1 Background

1.1.1 About Electric Propulsion

Chemical propulsion uses energy created by chemical reactions between a fuel and oxidizer to create thrust. Combustion heats the exhaust, which accelerates as it expands through the nozzle. While capable of producing enough thrust to launch rockets out of our atmosphere, chemical propulsion is incapable of achieving the specific impulse necessary for deep space missions with reasonable propellant mass fractions, and propulsion systems can be extremely complicated as well as costly.

Looking into alternative solutions that can improve the efficiency of space travel, electric propulsion (EP) comes into play. Electric Propulsion offers higher specific impulses, which it achieves through the use of the Lorentz Force and electrical heating of gases [4]. With more thrust for significantly less mass, the spacecraft will be much lighter, and the reduction in propellant would result in huge cost savings.

1.1.2 MPD Thrusters

One form of electric propulsion being developed is the magnetoplasmadynamic thruster (MPDT). Illustrated in Figure 1.1, it accelerates plasma electromagnetically, using

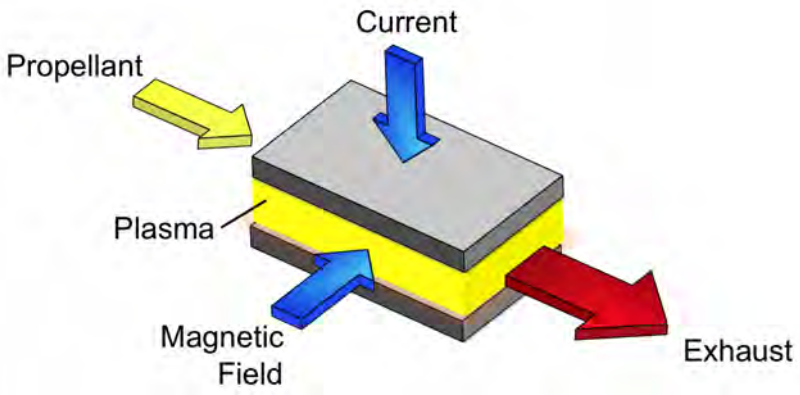

Figure 1.1: Electromagnetic Propulsion.[6]

high currents and both self-induced and external magnetic fields to generate a Loretnz force. These forms of thrusters generally consist of an ionized gaseous material that is pumped into an acceleration chamber. The ions are then accelerated out through the exhaust by the Lorentz force from the current flowing through the plasma and the magnetic field. [4]

The advantage of the MPDT over other forms of EP is its ability to process high mass flow rates through a compact device, resulting in a high thrust density, while maintaining high specific impulses characteristic of EP [4]. Depending on the magnetic field these MPDTs can either be Self-Field (SF) and/or Applied-Field (AF). In the case of SF-MPDTs, the magnetic field used is directly generated from the current that is traveling through the cathode. Although this design is simple, producing sufficient thrust would require MW levels of power -an amount far beyond the scale of current spacecraft power supplies (solar panels and RTGs). By applying an external magnetic field, AF-MPDTs are capable of operating in the 10s to 100s of kW -a level that is anticipated to become much more attainable in the near future [7]. The applied field acts to swirl the plasma, which generates thrust as the exhaust expands through the diverging magnetic field, converting the azimuthal motion into axial kinetic energy, and resulting in higher efficiencies. Lastly, the mass flowrate of the propellant is also a factor, as well as the pressure and area on which it is pushing (categorized as the cold gas component). Such thrusters are capable of extremely high Isps, up to 25 times the exhaust velocity of liquid rockets. Figures 1.2 and 1.3 illustrate the concept behind Self-Field (SF) and Applied-Field (AF) MPDTs.

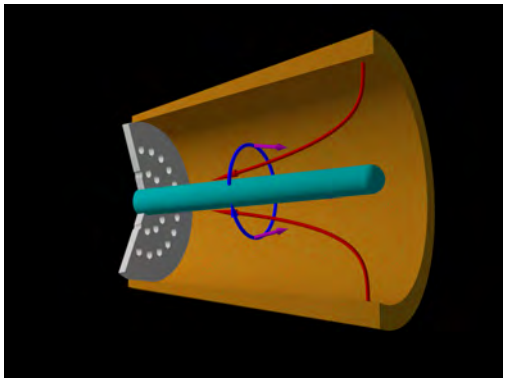

Figure 1.2: Diagram of a SF-MPDT with an annular anode and central cathode. The current is shown in red, the magnetic field is blue, and the cross product of the two is purple.[2]

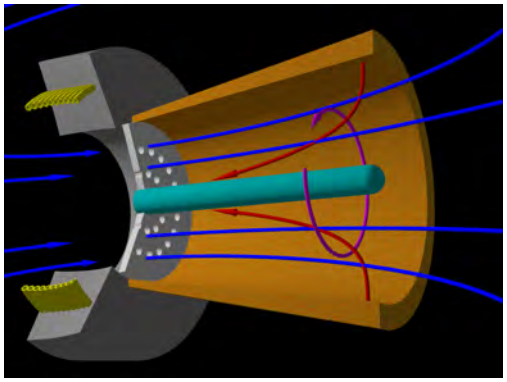

Figure 1.3: Diagram of an AF-MPDT, generated by the solenoid wrapped around the thruster. The current is shown in red, the applied magnetic field is blue, and the cross product of the two is purple.[2]

1.1.3 LiLFA

A variety of propellants have been used with Lorentz Force Accelerators, highest efficiencies have been achieved using lithium propellant. Lithium has a low first ionization potential (5.4 eV), meaning power is used in thrust generation, rather than ionization. Additionally with a relatively high second ionization potential (75.6 eV), there are reduced frozen flow losses due to secondary ionization. When barium is used as an additive, lithium also reduces the work function of tungsten (the cathode material), limiting erosion and thus increasing the thruster lifespan.

This type of MPDT, known as the Lithium Lorentz Force Accelerator (LiLFA), is an AF-MPDT, allowing for improved performance at lower power levels. Combining thrust from the Self-Field, Applied Field, and the cold gas component, the LiLFA is capable of achieving higher thrust densities than any currently flying electric propulsion device [2]. Coupled with a high specific impulse, this thruster is an ideal candidate for missions beyond low Earth orbit requiring short transit times, such as manned missions to Mars.

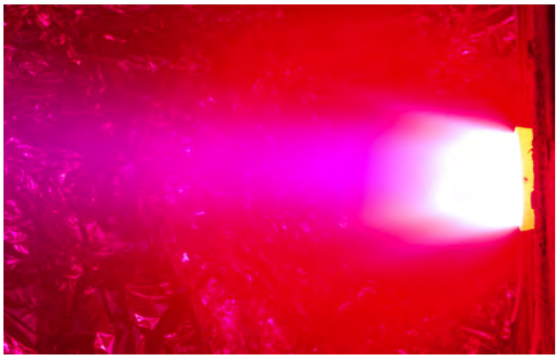

Figure 1.4: The LiLFA firing on May 7, 2015.[2]

Figure 1.5: Steady-State MPD Facility (Steel Tank) that houses the LILFA.[2]

1.2 Motivation

The LiLFA is currently being developed in the Electric Propulsion and Plasma Dynamics Lab (EPPDyL), where a large lithium-resistant stainless steel vacuum chamber houses all experimental testing (see Figures 1.4 and 1.5). To assist with ongoing research for the LiLFA, there has arisen the need to attain video documentation of the thruster operation in situ, downstream of the nozzle.

1.2.1 The Onset Phenomenon

One performance limitation of the LiLFA presently being investigated is called onset. When the mass flow rate of the propellant drops below a critical level, the thruster begins to self-erode. Microinstabilities arise in which bits of the anode material can break off, and the occurrence is characterized by large voltage oscillations. During onset, small electrical arcs can also form, tracing from the point of erosion of the anode radially into the cathode. However, there is currently no visual correlation between these events and the measured voltage oscillations in an MPDT using an applied magnetic field. With the integration of a video camera, we will be able to make this correlation between the two phenomena.

1.2.2 Testing Procedures

In addition to recorded footage for use as evidence, a camera will also facilitate testing procedures. As of now, it is difficult to obtain confirmation of propellant priming. A

researcher needs to look through a window at a mirror inside the vacuum chamber, which is angled to see inside the thruster nozzle. Then, from a considerable distance, he must obtain a visual of a small amount of liquid lithium pooling and dripping at the propellant entrance. This serves as a confirmation that the propellant has reached the acceleration chamber and that the thruster can be powered on. An in situ camera significantly lessens the distance to the thruster and allows for easy magnification.

Lastly, the integration of a camera will improve overall project documentation, creating more evidence of experimental testing and allowing researchers to confirm assumptions such as whether there is in fact an even distribution of propellant throughout the plume.

1.3 Project Description

1.3.1 Goal

The goal of this project is to design, build, and test a wireless video diagnostic system for the LiLFA. The system consists of a camera inside of a protective housing, with proper cooling built in. Appropriate power supply is needed for both the camera and any protective mechanisms. Lastly, the system must be able to communicate with researchers standing outside of the vacuum chamber, so that one can control the aforementioned mechanisms inside the housing, and for a live stream to be transmitted out to enable monitoring.

1.3.2 Challenges

The system must be designed for a variety of extreme environmental conditions that make this project particularly challenging. The camera housing must be able to withstand the high temperatures of the rocket plume, requiring both passive and active cooling to ensure that the camera itself remains within safe operating temperatures. Extending from this temperature durability is the fact that this camera must be able to operate within a vacuum, eliminating air convection as a possible cooling solution. Additionally, there cannot be any exposure to the reactive propellant that would compromise the safety of the camera. In order to eliminate the need for physi-

cal feed-thru's that can compromise the vacuum chamber, all communications needs must be met wirelessly and power must be supplied by rechargeable batteries for the duration of a typical experiment. Lastly beyond these fundamental mechanical design requirements, some innovation is required to maintain a constant visual. The propellant condenses on all surfaces it contacts. In other words, a molten lithium coating will continually block the field of view—a material that cannot be simply wiped away. A mechanism is needed to avoid the coating or continually remove it from the cameras view to allow for uninterrupted recording.

Chapter 2

Preliminary Design

2.1 Design Parameters

In order to begin the design process for this system, we must attain a better understanding of the environment in which the camera will be housed. Design parameters are then determined based on the position of the video system within the vacuum chamber. The primary engineering requirements include temperature and the mass flux of the lithium propellant.

2.1.1 Experimental Setup

As seen in Figure 2.1, the LiLFA is housed at the front of a large steel vacuum chamber of 1.5 m in diameter.the LiLFA is housed at the front of a large carbon steel vacuum chamber of 1.5m in diameter. The video diagnostic system will be positioned 2.41 m away from the anode and will be centered along the axis of thrust. This distance was selected so that the camera would be positioned toward the back of the vacuum chamber, allowing for a lower temperature environment, and the proximity to tap into the vacuum chamber's pre-installed cooling system. See Section 2.2.2 for more details. The position being alongside two of the eight optical ports of the chamber, a communication signal such as WiFi (2.4GHz frequency range and 12.5 cm wavelength) can easily pass through for wireless control and data transfer to researchers outside of the chamber.

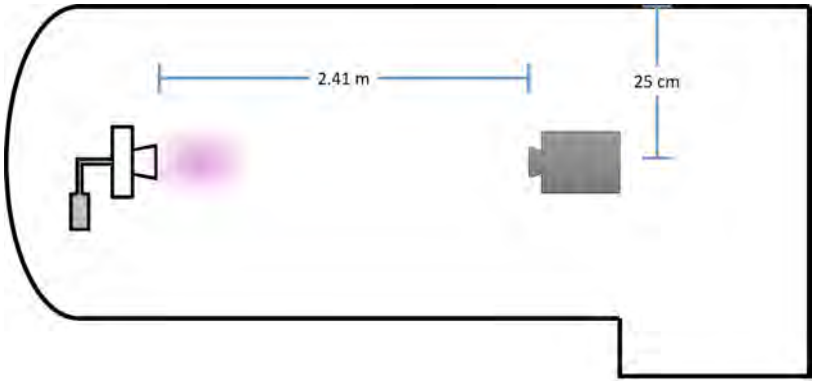

Figure 2.1: Cross-sectional diagram of the vacuum tank containing the lithium Lorentz force accelerator and the video diagnostic system.

2.1.2 Temperature

The temperature in this portion of the vacuum chamber was initially estimated from a prior experiment conducted by Coogan et al..[3] In their testing of the dynamic resistance probe, a K-type thermocouple was placed at a distance of 1.67 m from the tip of the anode and 23 cm below the axis of thrust. For the purposed of this design, the temperature at the location of the camera was assumed to be the same. After 500 seconds of thrust, the temperature was recorded to be 65° C and was increasing linearly throughout the data collection period. Assuming this temperature would continue to rise for several more minutes, all materials selected for the exterior of this system would be able to withstand a temperature of 100° C.

2.1.3 Pressure

Once the tank is fully pumped down, pressures reach a level on the order of 5 x 10 $^{-5}$ torr [3]. As a result of the vacuum, all components used in the system must not contain any oil or grease, as most lubricants will outgas. Any devices used, such as batteries, must be vacuum rated as well. Lastly any heat generating components will need to kept at safe operating temperatures in the absence of air convection.

2.1.4 Lithium Mass Flux

Applying the model detailed in Refs. [3] and [5], we can estimate the rate at which the lithium propellant condenses on the surface of the video system. This parameter

determines how much time is available before the visual of the thruster is lost.

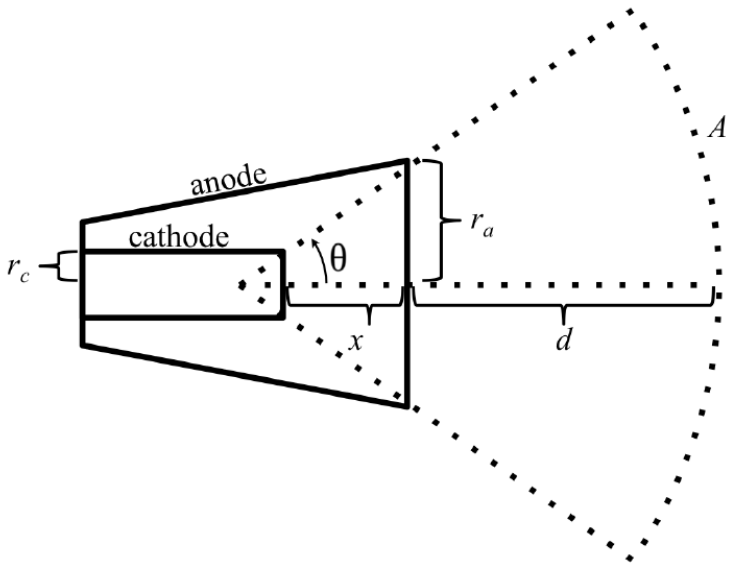

Figure 2.2: Cross-sectional diagram of the lithium Lorentz force accelerator. [3]

Figure 2.2 illustrates the layout of the LiLFA nozzle, and provides the reference geometry from which to approximate the mass flux as a function of distance d from the anode exit plane. Note that according to the desired position of the camera, the actual distance would be proportionately larger in the diagram.

The mass flux is given by

$$\Gamma = \frac{\dot{m}}{A}, \tag{2.1.1}$$

where $\dot{m}$ is the maximum operating mass flow rate of 20 mg/s and A is the area over which the mass is distributed at distance d.

Solving for A from the geometry given in Fig. 2.2, we find that

$$A = 2\pi(1 - cos\theta)(d + x)^2, \tag{2.1.2}$$

where x can be ignored when $d \gg x$. θ, the divergence of the plume, has been

observed to be approximately 30° [3].

Table 2.1: Measurements taken from the LiLFA

Parameter	Measurements
x	70±1 mm
r_a	35±1 mm
r_c	12.0±0.5 mm
d	2.41±.003 m

Using the measurements of the thruster setup provided in Table 2.1, the theoretical mass flux is found to be 0.386 μg/cm^{2}s. However, from previous measurements collected by the dynamic resistance probe, it was determined that the observed mass flux was approximately half that of the theoretical value. This factor was then used to approximate the actual mass flux as 0.176 μg/cm^{2}s.

It is important to note that this value represents a uniform mass flux throughout the cross sectional area. As the deposition rate is certainly higher at the axis of thrust than it is off axis, a distribution model is applied in which the mass flux decreases linearly with the radius of the cross section. For simplicity, the cross section of the plume is approximated as a circle as opposed to the arc seen in Fig. 2.2. Given this linear distribution, the mass flux at the axis of thrust, Γ', is twice that of the average value

$$\Gamma' = 2\Gamma. \tag{2.1.3}$$

Thus the lithium deposition rate in front of the camera is approximated to be 0.3511 μg/cm^{2}s. Slightly less than what was originally estimated by the model, this value is the maximum mass flux of the propellant onto the video diagnostic system.

This value can now be used to approximate the amount of time before visual of the thruster is lost by the accumulating lithium. Before this can be done however, we must determine the thickness of lithium that correlates to the transparency limit. For metals, this transparency limit is comparable to the skin depth

$$\delta_s = \sqrt{\frac{1}{\pi f \mu \sigma}}, \tag{2.1.4}$$

where δ_s is the skin depth (m), μ is the permeability (H/m), f is the frequency of light (Hz), and σ is the conductivity (S/m) [1]. Given the frequency range of visible

light (430 to 770 THz), the permeability of lithium ($4\pi * 10^{-7}$ H/m), and its bulk resistivity (reciprocal of conductivity; 9.29 $\mu\Omega \cdot$ cm), this skin depth is approximately 50–60 angstroms. Thus 90% transparency must be on a comparable scale on the order of 100 angstroms.

Using the density of lithium (0.512 g/cm^3), one finds that the mass flux at the camera correlates to a thickness rate of 68.59 Å/s. With a transparency limit of 100 Å, this equates to only 1.458 seconds before visual of the thruster is lost. As a result of this extremely short time span, letting lithium accumulate in front of the camera is not an option. A protective lens cannot simply be cleaned off between trials. There must be an active method for keeping the line of sight of the camera lithium-free. The solution developed will be addressed in Section 2.2.4.

2.2 Alternatives Analysis

The following section provides an overview of the preliminary design choices given the experimental setup and the parameters defined above. It is worth noting here that several design alternatives were considered before pursuing the concept of a camera within the vacuum chamber. The most straightforward solution would be to position a camera outside of the tank, pointed directly at the thruster. While possible in other tanks in the EPPDyL, the pumps and cooling pipes at the back of the steel tank prevents this option. It was then considered that the camera could be positioned outside of a side window, with a mirror positioned in the tank for visual of the thruster. However, such a mirror would constitute an even larger surface area on which lithium would coat when compared to the camera itself. Solutions to maintain visual in spite of the condensing propellant, discussed later in this chapter, would become even more challenging for a mirror. Other proposed concepts included designing fiber optic feedthrough, which would limit the number of electronic components under vacuum. While still facing the same issue of the lithium coating, this solution would come with complications of its own, including the risk of a leak when installing an additional feedthrough in the tank. Among the options considered, a small camera that could capture high resolution footage through clear and direct exposure to the plume was determined to be the best solution.

2.2.1 Camera Selection

A variety of cameras were considered for the video diagnostic system, primarily adventure or "action cams" due to their compactness and durability in withstanding extreme environments. These cameras often tend to have built-in Wi-Fi connectivity, allowing for convenient wireless communication with personnel monitoring the LiLFA. The only setback to these cameras is that they tend to record at a fixed wide-angle focal length. With the system being positioned 2.41 m away from the thruster, a lens with telephoto capabilities would be ideal.

While no camera comes with a built-in telephoto lens, a model with an interchangeable lens could meet the necessary requirements. DSLR's tend to be rather bulky, but mirrorless cameras being developed in recent years are much more compact and tend to have built-in wireless communication. After researching, the mirrorless camera regarded as the "best performer" in terms of meeting these design requirements is the Z Camera E1, a compact 4K video camera with a Micro Four Thirds lens mount. With the proper telephoto lens attached, this camera would be capable of obtaining high resolution footage of the LiLFA despite the distance apart. The only drawback to such a camera is the price range. The E1 camera itself costs $700 as of January 2017, with suitable focal length lenses in the $300–$700 range. For a product that has never been tested in such extreme environments, the E1 camera is a risky investment.

Figure 2.3: 2016 GoPro Models.

Upon further review, the GoPro Hero 5 Session was selected as the optimal camera for the system. Unlike other action cameras, the GoPro series has included several different Fields of View (FOV): Wide, Medium, and Narrow. As the lens is fixed, these settings do not change the focal length, but crop the image to create the same FOV. As a result, a 4K resolution in "Narrow" mode crops the view to a 1080p segment of the overall frame. While certainly a step down from a 150 mm focal

length at 4K that the E1 camera could provide, a Narrow FOV GoPro recording at 1080p with a focal length equivalent of 34.4 mm is certainly sufficient for diagnostic and documentation purposes, at a much more reasonable price. Furthermore, there is substantial documentation of GoPro's being successfully tested in vacuum, making it a much less risky investment. Should the camera be recording for an extended period of time without cooling or should the cooling system fail, GoPro's are programmed to automatically power off at temperatures that exceed 68° C.

Compared to other GoPro models, the Hero 5 Session was selected for its compactness and cost. While other larger models include features such as touch screens, these attributes would not be used within a vacuum chamber (only leading to greater risk of overheating), and are not worth the added cost and size. While maintaining the same resolution as these models, the Hero 5 Session is the most compact and cost effective at $300, making it the optimal choice for the system.

2.2.2 Cooling Method

With air convection being nonexistent within the chamber, electronics such as the GoPro, batteries, and the microcontroller can overheat under vacuum alone—not to mention the extreme heat from the thruster. To limit the amount of heat from the thruster, a heat shield is mounted in front of the system. A thin plate protecting all components from the plume, the shield is separated via screws and machined out of steel due to its low thermal conductivity, thereby minimizing heat transfer over to the rest of the system. As an opening in the steel plate is needed to maintain visual, further protection mechanisms for the camera are discussed in the following sections.

For preventing overheating of the electronic components due to internal heat generation, heat transfer via conduction was chosen over potential convection mechanisms. While branching off from any preexisting water cooling lines may be possible, it is prone to leaks in practice. As a result, it was determined that the system would be best cooled via conduction through a metal block to the cooling system located in the back of the vacuum chamber. Although copper was initially considered for its high thermal conductivity, aluminum was selected as it is much less costly while still maintaining a sufficiently high thermal conductivity. The camera, batteries, and microcontroller are all attached to this block. Sizing of the block via a heat flux analysis is carried out in section 3.1.7.

2.2.3 Shutter & Filter Mechanisms

As video footage of the LiLFA may only be needed for certain portions of the duration of the thruster firing, it is advantageous to have a shutter mechanism to protect the camera from the lithium plume when not in use. Additionally, the light from the thruster is far too bright for any camera to record without the footage being dramatically overexposed. A material such as welding glass would therefore be able to block enough light to correct for this, but it should not be permanently fixed in front of the lens. When using the live feed to identify propellant priming before firing the thruster, one would need all available light. As a result, the filter should also have an "on" and "off" position like the shutter, and the same mechanism may be used for each.

The primary requirements for such a mechanism are compactness and low power draw. While making the system a compact box is ideal for portability, the space can be certainly be slightly increased to accommodate a larger than anticipated shutter and filter if need be. Thus the driving factor is power consumption, as the system will run on batteries as to avoid extra feed-through wires in the vacuum chamber. Though many methods for actuation are pneumatic, these could not be used under vacuum due to out-gassing. Strictly mechanical options may also be challenging to implement. As a result, electrical solutions are best suited to meet the design requirements. Ideally, the mechanism selected would be binary state with zero current draw in both the open and closed positions, and minimal power to switch between them. A variety of technologies were considered for this function and are outlined below:

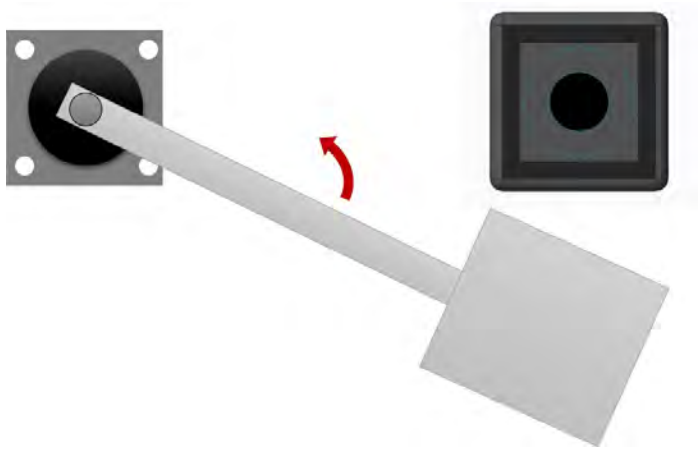

Figure 2.4: Motor-based shutter mechanism concept.

Motors

Several types of motors were evaluated for the task, with the idea that the rotational motion could be used to move the shutter away from the lens. The shutter, a thin plate of steel, would then be attached by a rod to the motor shaft. Stepper motors were initially researched for their ability to conveniently handle position control. However, while one can design the system such that the "off" position is shutter-closed, the motor would constantly be drawing power to remain in the shutter-open position for the duration of the recording.

One solution proposed to maintain the shutter-open position without drawing power was to use the stepper motor in conjunction with a worm drive. The gear configuration would then hold the motor in the shutter-open position even when the motor is powered off. To return to the closed position after recording, the motor would simply spin around until the shutter piece is once again in front of the lens. While this system certainly meets the design requirements, it is a little more on the complex end and could cause difficulties in implementing if the gears do not align as intended. It is also worth noting that the configuration would also significantly reduce the opening and closing speed. Lastly, the setup would require additional space due to the non-reversibility of the gear configuration. The motors alone cost on the order of $50–$100.

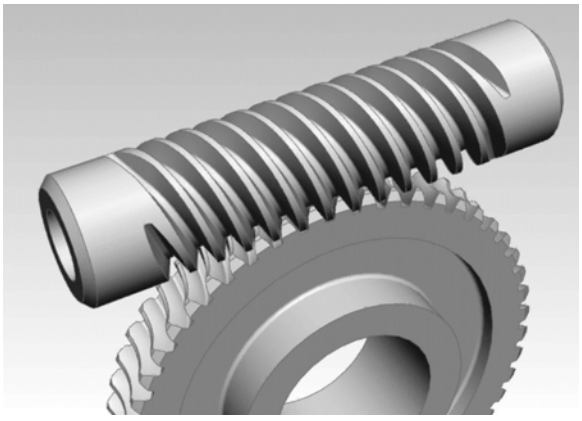

Figure 2.5: Worm Drive mechanism.[9]

Although not traditionally used for position control, basic DC motors were also considered for this application. It is possible to integrate these with a stopper at the open and closed points, to avoid timing issues in which the motor would spin past the desired position when powered. To keep the shutter in place when the motor

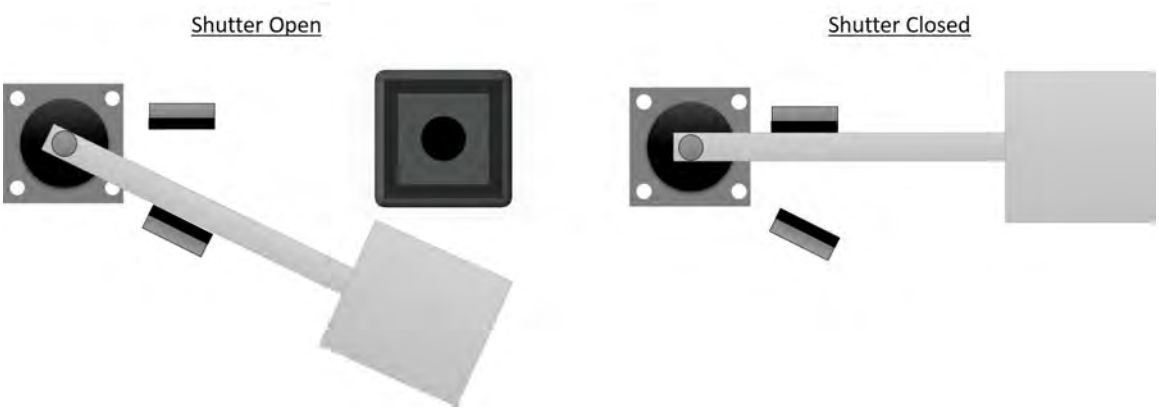

Figure 2.6: Shutter powered by DC motor with magnetic stoppers.

is powered off, especially if there are some recoil effects from the shutter hitting the stopper, magnets should also be included to keep the rod in place. This method could be used for stepper motors in addition to normal DC motors, as long as the motor in either case is bipolar to allow the shutter to reverse direction between the two stoppers. Compact square-face DC gearmotors, best suited for the system over other motors in terms of relatively low rpm and their square shape for easy mounting, are priced at approximately $50.

Solenoid Actuators

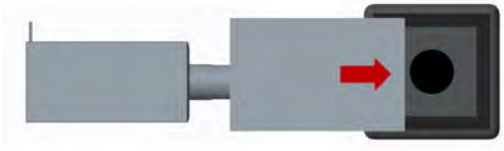

Figure 2.7: Solenoid Concept (Slider)

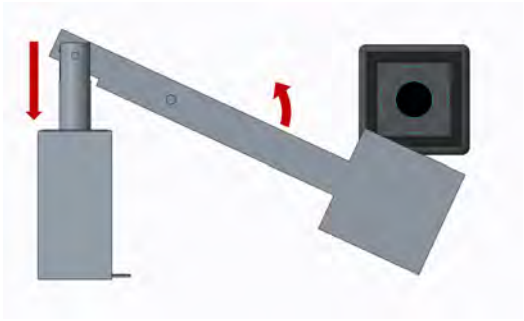

Figure 2.8: Solenoid Concept (Pivot)

While some of the motor-mechanisms appear to be plausible solutions with the potential for zero-power consumption in both the open and closed states, a technology that is designed specifically for binary state positioning may be much more ideal. This need can be met by a linear solenoid actuator. A compact device, the actuator switches from a resting position to an extended or shortened position (depending on whether the type is "push" or "pull"), when current is applied. Depending on the

length the plunger can extend, the actuator may be able to slide a shutter or filter piece directly in front of and away from the lens (Figure 2.7). If the extension distance is not long enough, a pivot may be used instead (Figure 2.8). Unfortunately, to maintain this current-activated position, power must be continuously drawn.

In order to use a solenoid actuator while preventing zero-current draw in each state, a mechanism would be needed to hold the plunger in place when in its active state. One such method that was considered was a spring mechanism, such that the plunger would be held in place by the spring tension. However, as this may lead to some difficulty with finding a spring with the appropriate stiffness, a strong magnet was determined to be a more reliable method. Upon further research, several suppliers of what is known as a magnetic latching solenoid were discovered. These devices contain an internal magnet that the plunger latches to in its active state. As power is no longer required to maintain this position, only current draw from the battery occurs when switching state—a rather infrequent and low-power activity. At just over $30, these magnetic latching solenoids were determined to be the simplest and most cost effective solution. Further details on the product sizing and the way in which these solenoids were implemented will be provided in Chapter 3.

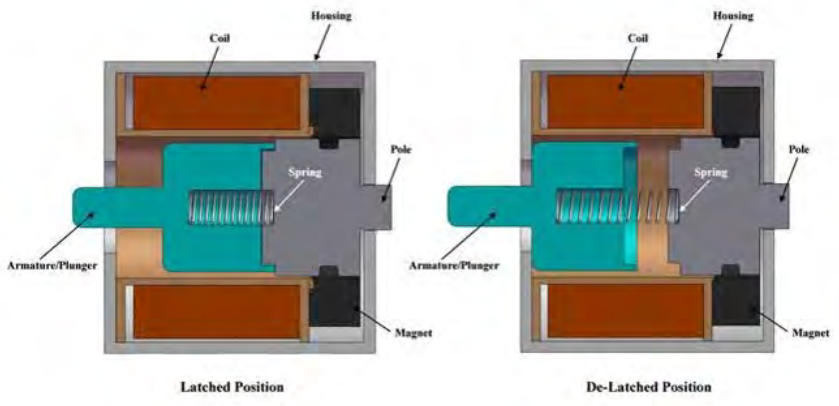

Figure 2.9: Schematic of a Magnetic Latching Solenoid Actuator [8].

2.2.4 Maintaining Constant Visual

One of the most significant challenges in terms of obtaining footage for any duration of time is the issue of the condensing lithium being deposited on the camera. With

a delay of only 1.5 seconds before visual is lost according to the model presented in Section 2.1.4, a mechanism needed to be devised that would prevent the lithium from accumulating to that extent.

Several potential methods were discussed among the lab group, ranging from electromagnetic to purely mechanical mechanisms. Deflecting ions away via a magnetic field was suggested, but the plume would actually consist of a mix of positive and negative ions, and the field may not be strong enough to deflect particles flying head on at such a high velocity. If the propellant was allowed to accumulate on the protective glass in front of the camera, it is plausible that heating up the glass can melt the lithium away. Unfortunately, this is not likely to be as clean of a solution in practice, as the lithium may simply streak, and would be difficult to remove entirely before a new layer accumulates.

If deflection and removal are not achievable, a disposable surface on which the lithium can accumulate was determined to be the ideal solution. This surface would need to be transparent as it will be placed in front of the lens, but also needs to be continually moved or swapped due to the small amount of time before the lithium accumulates to the visual limit. The mechanism devised for this problem is a scrolling roll of transparent Mylar, powered by a DC motor. The portion of the Mylar that is not directly in front of the lens will be protected from the plume by a shield, so that a clean sheet can be continuously scrolled in front of the camera to prevent lithium accumulation.

2.2.5 Remote Power On

Due to prolonged inactivity while researchers are preparing the tank for thruster firing, the GoPro will most likely switch from standby mode to full power off. When this occurs, the camera can no longer be activated via WIFI alone. The power button on the device must be physically pressed.

It was conceived that it may be possible to carry this out electrically, removing the button and connecting a relay to the PCB inside in order to temporarily complete a circuit that emulates the pressing of the button. Unfortunately, implementation of this idea was more challenging than expected. Due to waterproof sealing and overall compactness, disassembly of the GoPro is irreversible and prone to damage, and the very small components of the circuit boards within would be difficult to solder a

connection onto. As a result, it was decided that it would be less risky to keep the camera intact. To physically push the button, a solenoid actuator was again used, mounted behind the camera with a protruding piece at the height of the button, and a small gap to allow motion for sufficient impact.

2.2.6 Communication and Controls

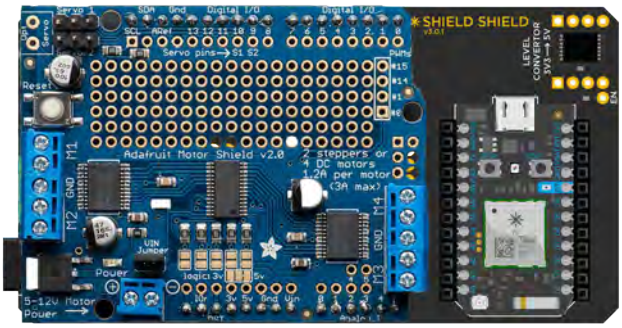

Figure 2.10: Microcontroller and Motor Shield Configuration.

When selecting a control system, the driving design requirement was wireless communication. Based on compactness, affordability, and familiarity from use in previous lab courses, the Particle Photon was selected as the microcontroller for the system. As the Photon itself can handle up to 5V, a method was needed to channel a higher voltage to control the 12V motor and actuators, along with the ability to reverse polarity. After researching similar cases of motor control, it was determined that the simplest solution to achieve this are H-bridge chips. The Adafruit Motor Shield v2.3 elegantly handles this, with enough slots to power both the solenoids and the Mylar scrolling motor. The shield is also compact enough to fit within the limits of the box, the size is comparable to that of a half size bread-board. To use this with the Photon the Particle Shield Shield adapter is needed, which sits flush with the motor shield.

2.2.7 Power Sources

As the GoPro and Photon are both USB powered, it was convenient to simply use a USB battery bank sized for the GoPro recording time. These batteries are typically

lithium-ion, and are quite affordable due to their recent mass production for cell phones and tablets. Upon purchase, the battery bank was then tested in vacuum while discharging, to ensure successful operation. With no damage to the battery after a series of tests, it appeared that li-ion batteries can indeed meet the design requirements, as long as they are properly cooled. While an appropriate 12V li-ion battery could not be found to power the motor and solenoid actuators, a Sealed Lead Acid (SLA) of sufficient capacity was selected instead and successfully tested in vacuum. Further details on the power supply, particularly the energy consumption modeling that led to the battery sizing, will be included in Chapter 3.

2.2.8 Housing

Plastic may not provide sufficient structural integrity under extreme temperatures. As a result, a metal such as aluminum would be a more suitable material for the conditions while remaining relatively machinable for the manufacturing of various components. The camera would be housed in a box like structure, with the various mechanisms being mounted to the walls. Heat generating items such as the Photon, batteries, and of course the GoPro itself must maximize contact with the cooling block, which extends out of the box to the aluminum mounting bracket.

Layers of Protection

To provide an overview of the placement of protection mechanisms for the GoPro, the following list reflects the order from direct contact with the plume to right before the camera:

1. Heat Shield - Protects box but has portal for the camera.
2. Shutter - Protects camera when not recording.
3. Mylar - Scrolls in front of camera. Only the portion not covered by the heat shield is exposed to the lithium plume.
4. Glass - In case the Mylar is damaged, a small glass window will be placed in the wall as an extra layer of protection.
5. Filter - While the thruster is firing, a filter will be needed to correct the exposure.

6. GoPro - Already designed for rugged environments, the GoPro has a replaceable glass lens cover of its own.

With all of these mechanisms installed, the LiLFA video diagnostic system provides more than sufficient protection for the camera while maintaining a clear view of the thruster.

Chapter 3

Detailed Design

3.1 Component Selection and Design

The following section provides a walk through of the design decisions for each of the major components of the LiLFA Video Diagnostic System.

3.1.1 Heat Shield

Figure 3.1: Heat Shield mounted on camera housing [CREO Rendering].

The primary layer of protection in the system, a steel heat shield is mounted in front of the camera housing. Given that the front face of the system is 8" x 8.5" (see Section 3.2.1 for housing sizing), a 10" x 10" piece of 1/16" General Purpose Low-Carbon Steel was selected for the shield as it sufficiently covers the system from head on contact with the lithium plume. While steel was used for its low thermal conductivity, the shield will also be suspended 3/4" away from the system via six 6-32 steel screws to further prevent heat transfer to the rest of the system. The 1/16" thickness was selected as it provides sufficient structural rigidity while remaining light enough to be suspended from the screws and not provide a torque on the camera housing.

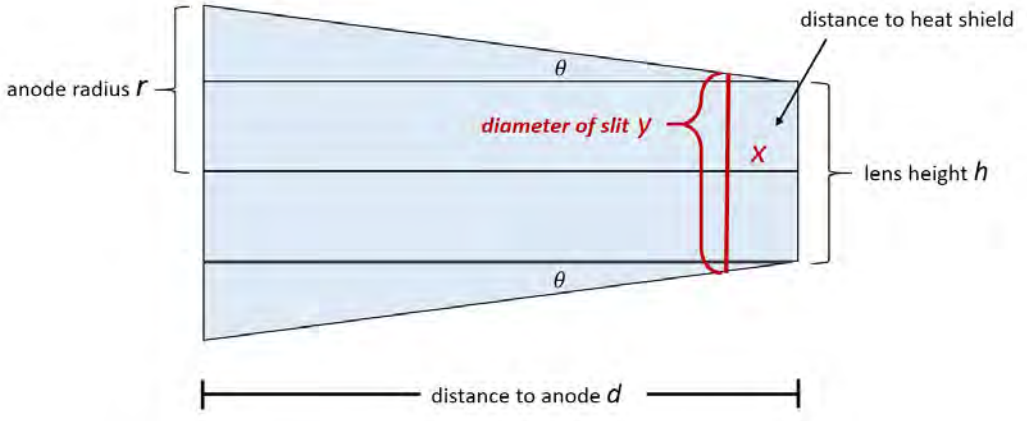

Figure 3.2: Schematic for minimizing heat shield slit size.

In addition to the six screw holes, the shield must also have an opening for camera visual. A circular hole was cut for ease of manufacturing via CNC milling, and was initially sized according to the radius of the thruster anode. As shown in Figure 3.2, the difference between the anode radius (r = 1.38") and the radius of the lens ($h/2$ = 0.25") will determine the minimum necessary field of view. With a small angle increase of $\theta = 0.681°$ due to the 7' 10.88" distance to the anode, the diameter of the slit located only 2.2" away from the camera must be at least 0.55".

While a 0.55" wide hole would allow for a view of the anode, it was decided by the lab group that it would be beneficial to capture more of the vacuum chamber. A wider range of view would be able to capture more of the plume, especially if the thrust vector were to rotate away from being directly in line with the camera. For the final design, the field of view (FOV) of the GoPro lens itself was used for sizing the opening. With a vertical FOV of 37.2° in Narrow mode, a heat shield opening of

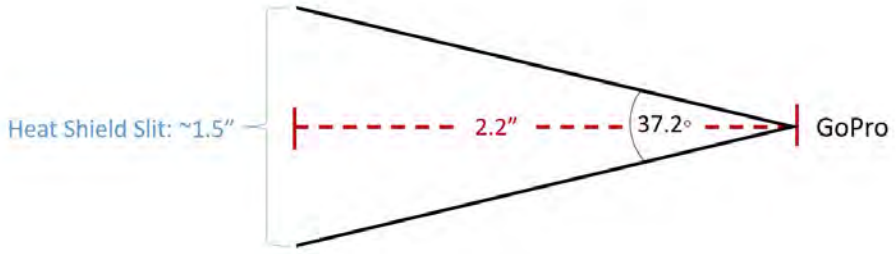

Figure 3.3: Sizing heat shield slit from GoPro FOV.

1.48” would allow for a full view from top to bottom. This was rounded up to a 1.5” diameter hole for clearance.

3.1.2 Mylar Scrolling Mechanism

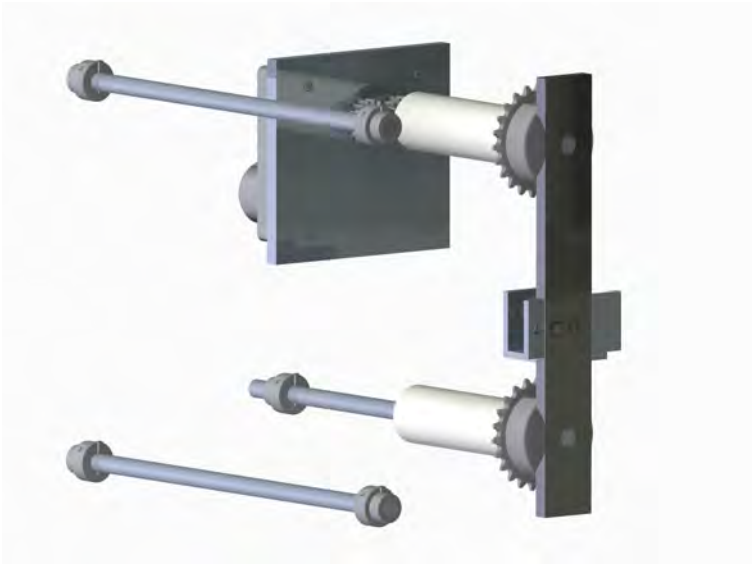

Figure 3.4: CREO Parametric model of Mylar Scrolling Mechanism.

The Mylar scrolling mechanism consists of a motor and four shafts, as seen in Figure 3.4. A square-face DC gearmotor was selected to drive the scrolling as it is easily mountable, compact, and meets the required specifications. Connected to a shaft through a gear coupling and linked to the shaft below it via a chain-sprocket configuration, the top and bottom shafts rotate to scroll the Mylar at the speed of the motor.

Demonstrated in Figure 3.5, the film will be stored in position I, and scroll in front of the camera and upwards, wrapping around a dowel at position IV. To allow for

the motor and rolled film to be housed within the protective housing, shafts II and III are needed to bring the Mylar outside of the box, in between the camera and the shutter.

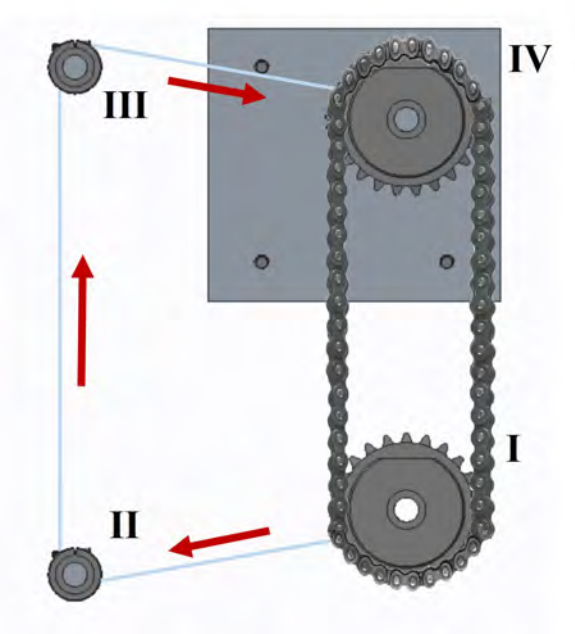

Figure 3.5: Mylar Scrolling Schematic (Profile View).

While controlling the rotation of the bottom shaft via the chain drive is ideal for loading the Mylar into its storage position, it is not meant to be active while the film is being scrolled in front of the camera. With the majority of the film is stored at position I at the start of a run, the radius of the dowel is effectively larger. For a significant portion of the run, the feed rate from the bottom shaft would be higher than the intake rate from the top shaft, causing the film to scroll out in a disorganized and untensioned manner. Therefore after loading the film onto the bottom shaft via an external roll, the researcher should loosen the set screw on the top sprocket, disabling the chain drive. The bottom shaft will then only spin at the rate the top shaft is scrolling the Mylar, enabling the film to be tensioned throughout.

Motor Selection

Given the maximum time span of 1.458 seconds before visual is lost, the motor for the scrolling mechanism needed to be sized appropriately. To maintain clearer visual, the time is rounded down to $t = 1$ s.

With an exposed length of $L = 1.5$" due to the hole in the heat shield, this would mean that the mylar in front of the camera must scroll at a rate of $L/t = 1.5$ in/s. As 1" (circumference $c = 3.14$") plastic dowels were used to hold the mylar, these must spin at a rate of at most $(L/t)/c = 0.477$ rotations per second or 28.65 rpm. While this rate can be decreased with an increasing radius as more mylar is scrolled, it is best to size the speed for the worst case scenario.

For compactness, easy mounting, and to avoid the complications of a custom gearing down of a DC motor, a square-face DC gearmotor from McMaster-Carr was selected for the system. Of the available speeds, the 50 rpm version was selected as it was safely above the minimum required speed, while allowing for flexibility by adjusting the PWM signal of the microcontroller. This buffer would enable the system to be adaptable to deviations from the original design parameters, for example, in the case that the mass flux model used in section 2.1.4 proved inaccurate, a higher propellant mass flow rate is ever used when firing, or the battery was not fully charged.

Scrolling Mechanism Configuration

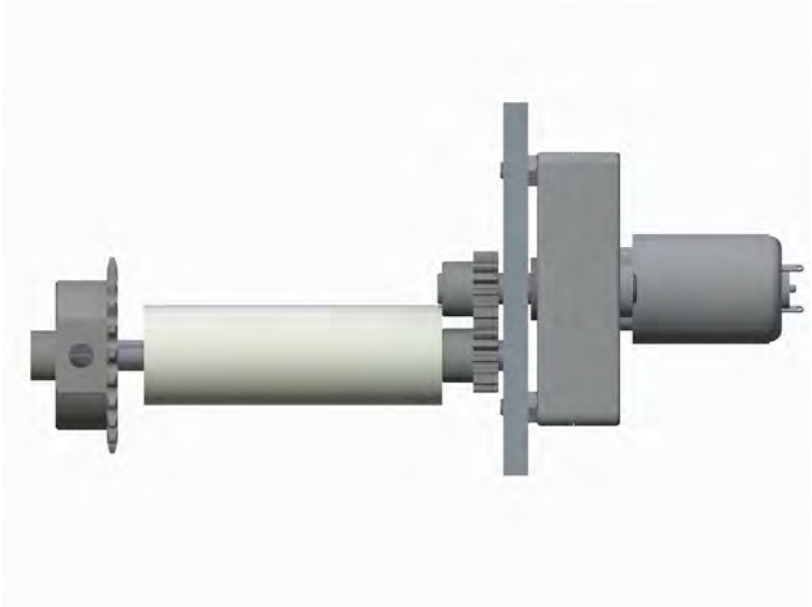

Figure 3.6: Top down view of motor mount and gear coupling. [CREO Rendering]

The shaft connected to the motor and the one directly below it are both fitted with 1" plastic dowels around which the Mylar will wrap, and steel sprockets linked by an ANSI 25 stainless steel chain. To ensure that the dowels would withstand heat

transfer from Mylar exposed from the lithium plume, Extreme Temperature PTFE was selected for the application, with a range up to 260°C. While the heat shield opening is only 1.5" wide (see section 3.1.1), the film was cut to 2.5" in length to allow for more structural integrity around the section that is exposed to the lithium plume. As a result, the plastic dowels were sized to be 3" in length to allow sufficient room for the Mylar to wrap around them when loading and scrolling.

As shown in Figure 3.6 The motor is mounted onto a 1/4" aluminum plate, and connected to the first of the shafts through an equal diameter gear pair. As the built in motor shaft is 5/16," a 5/16" rod was used for all other shafts for simplicity when manufacturing. Each of the shafts were fitted with dry running sleeve bearings, as any lubricant would raise the pressures in the vacuum chamber.

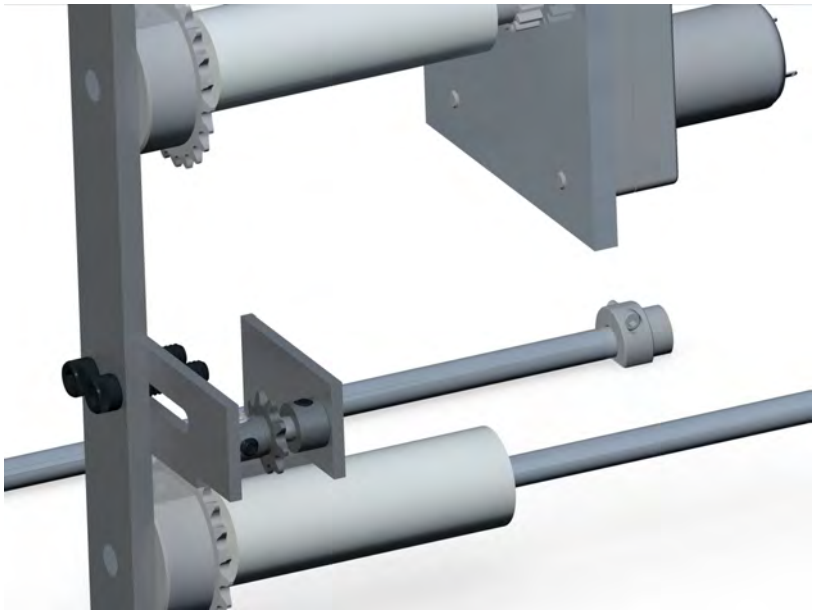

Figure 3.7: Chain Tensioner Assembly. [CREO Rendering]

Lastly, a tensioner was needed as the chain was not a perfect fit for the distance between the two axles (this distance was determined by the spacing requirements of the housing). The tensioner would ensure that the chain would remain secured onto the sprockets through repeated usage. A 1/8" aluminum U-channel was cut to a sufficient length of 3", allowing for a 1.75" long slot for adjustments when tensioning. The tensioner is supported by two 1/4"-20 bolts, and is secured in place by lock nuts when the correct position is achieved. At the end is a 1/4" D-profile shaft with an ANSI 25 idler sprocket to support the chain, and a shaft collar to prevent the shaft from sliding through the bearings. The tensioner assembly can be viewed in Figure

3.7.

3.1.3 Filter Mechanism

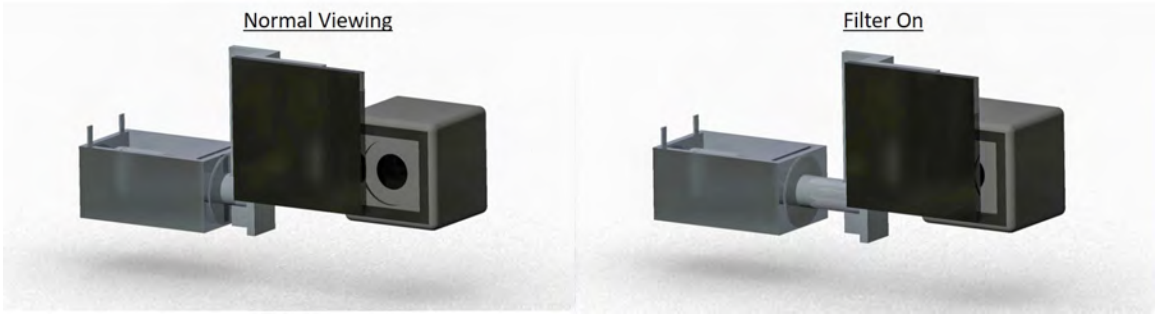

Figure 3.8: Filter mechanism [CREO Rendering].

As discussed in Chapter 2, a solenoid actuator was determined to be the best solution for both the filter and shutter mechanisms as it allows for simple binary state positioning with zero power draw to maintain either state. Looking at commercially available magnetic latching solenoids, the following parameters drove the final selection:

- Stroke Length: As the gopro lens is 1/2" in diameter (and the overall front face is 1.5" in diameter), the solenoid should extend sufficiently far to clear this distance.
- Duty Cycle: Continuous; the solenoid should be designed to remain in either state for extended periods of time, as opposed to a pulsed solenoid which occupies the extended state for very minimal periods.
- Voltage: 12V; as the DC gearmotor selected for the Mylar scrolling mechanism runs at 12V, a uniform voltage would facilitate power sources and their connection to the microcontroller.

The Pontiac Coil Inc. G0411A was ultimately selected as it meets these criteria with the largest stroke length of 0.75." This distance is sufficient enough to clear the lens of the GoPro if the filter is placed directly in front of the camera. Figure 3.8 portrays the sliding mechanism made for this purpose. The filter, cut from a plate of welding glass, is supported by an 1/8" aluminum holder that runs along the side and top portion of the glass, and is secured via an epoxy rated for high temperatures. The holder is screwed onto the solenoid actuator, which then pushes it out far enough to

cover the entirety of the lens. Upon testing several shades of welding glass, Shade #6 glass was selected for the optimal exposure of the plume.

3.1.4 Shutter Mechanism

Figure 3.9: Shutter mechanism [CREO Rendering].

Apart from the heat shield, the shutter is the only other component in the system that will face long term exposure from the lithium plume. As such, the piece was machined out of steel for its low thermal conductivity. To accurately protect the portion of the system exposed through the opening in heat shield, a 1.5" x 1.5" shutter is needed.

With the shutter being placed in front of the filter, the protective glass, and the scrolling film, it is sufficiently separated from the camera that a slider mechanism would not suffice. Given the GoPro's field of view, the shutter would have to extend further than 0.75" away from the camera to be clear of the shot. As no solenoid actuators available with stroke lengths beyond 1", a pivot mechanism was implemented for the shutter using the same type of actuator as the filter.

A CREO rendering of the mechanism is shown in Figures 3.9 and 3.10. The solenoid actuator, vertically mounted, is attached to the shutter via a rod sliding along a slot in the shutter piece. The slot, paired with the pivot point, enable the shutter to rotate with the vertical motion of the solenoid. The length of the slot also determines the stopping point of the rotation, enabling a 20 degree rotation of the shutter to ensure a clear view when opened. As the 1.5" width of the shutter is an unnecessary amount of steel for the unexposed portion, it is connected to the solenoid via a 1/2" wide bar.

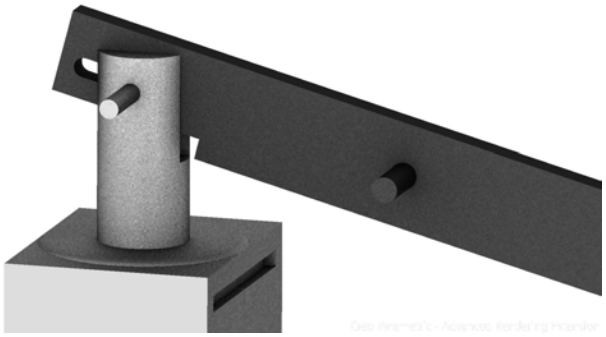

Figure 3.10: Close up view of attachment for shutter mechanism [CREO Rendering].

Using a similar triangles relation, one can find the position of the of the pivot point necessary to achieve the clearance for the 1.5" shutter. Using Figure 3.11 as a guide, one has the following initial parameters:

Table 3.1: Shutter Pivot Parameters

Parameter	Symbol	Measurements
Solenoid Maximum Height	$Y1$	0.6"
Shutter Clearance Height	$Y2$	1"
Length of Bar	L	4.3"

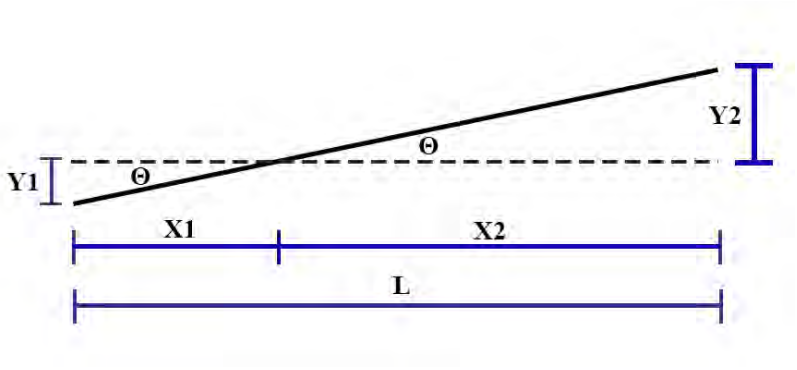

Figure 3.11: Pivot point calculations for solenoid actuator based shutter mechanism.

While the solenoid actuator selected is capable of a stroke length of up to 0.75", the amount of force lowers with increased length. When testing, it was discovered that the actuator could not pull in at its full extended length on a horizontal surface, let alone under a torque from the shutter. As a result, capping off this extension at $Y1$ = 0.6" would help ensure a return to the shutter closed position. At this length, the

associated force for this device is approximately 5 ounces. Sizing so that the left-most portion of the shutter is out of the field of view, the clearance height $Y2$ was safely set to 1" instead of the minimum 0.75" that would clear the lower half of the shutter. Lastly the length L, representing the distance between the solenoid and the shutter, is set to 4.3" as determined by spacing requirements in the housing (see Section 3.2.1: *Camera Housing* for more details on solenoid positioning).

$$X1 = Y1\frac{L}{Y1 + Y2} \tag{3.1.1}$$

According to this calculation, the pivot point should be approximately 1.61" away from the solenoid and was machined accordingly. Remaining 5/16" steel rod was used to construct the pivot, and shaft collars were placed on both sides of the bar to ensure a fixed rotation.

Given this pivot point, moments were calculated to ensure that the solenoid would be strong enough to achieve the desired motion. Using 1/16" thick steel, the moment about the pivot point is well within the capabilities of the shutter (5 ounces).

3.1.5 Remote Power On Mechanism

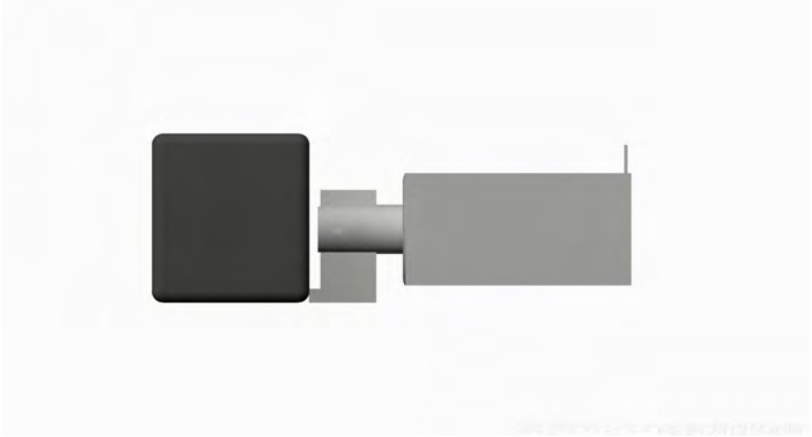

Figure 3.12: Remote power-on mechanism [CREO Rendering].

As the GoPro may power off after long periods of inactivity, a mechanism was devised to remotely power it on via communication with the Photon. At first, it was proposed that this may be feasible electrically. As buttons connect a conductive strip to complete a circuit when pressed. It may be possible to remove the button, and

connect two leads directly to the PCB underneath. These wires would be connected to a relay, which when temporarily activated would complete the circuit much like a physical button would.

Unfortunately, given their waterproof nature and overall compactness, GoPro cameras are not easily taken apart. Any part of the casing removed is permanent, and the intricate combination of PCB boards are located below a piece of plastic that needs to be sawed through. Furthermore, the underlying button on the PCB is extremely small, and would have been quite the challenge to remove let alone solder wires in its place. During the procedure to take apart this camera, one of the PCB boards was damaged, rendering the camera unusable.

While a relayed connection may have been a more elegant and error proof solution to the remote power on issue, it was decided that mechanically pushing the device's external button would be a safer approach. To do so, a solenoid actuator was once again used for the pulsing motion, and a small piece of aluminum was machined to to be mounted at the end of the solenoid for physical contact with the button. As shown in Figure 3.12, the actuator would be secured directly behind the camera, as the on button is located at the bottom center. The solenoid was mounted in such a way as to minimize the distance to the button, as the force of the solenoid would be significantly higher for smaller strokes. Testing the concept with the solenoid used for the filter and shutter mechanisms, it was determined that the particular model allowed for sufficient force for pushing the button. As such an additional one was ordered for this purpose.

3.1.6 Power Supply

The power supply for the video diagnostic system consists of two batteries, a USB battery pack to power the Photon and charge the GoPro itself, and a 12V battery to power the Mylar scrolling motor and the solenoid actuators.

The USB battery bank allows for plug and play connection to the GoPro and Photon, while the motor and solenoid actuators are all wired to the Adafruit Motor Shield, which is directly powered by the separate 12 battery. While all devices could theoretically be powered from the same source as long as the voltage is split and stepped down appropriately, using two separate batteries is a safer method and avoids complications that may arise with circuit design.

USB Battery Bank - Sizing & Selection

The following table summarizes the specifications of the two USB powered devices. While the Mylar may only be scrolling for 30 minutes, the GoPro itself may be powered on for much longer. During typical startup procedures, a researcher would power on the GoPro and connect with the smartphone app in preparation for firing the thruster. However, a successful firing may take several hours to achieve, during which the GoPro will remain connected to the smartphone on each attempt. As a result, the GoPro must remain charged throughout, and so the consumption was sized for a period of 6 hours.

For the Photon, however, this period of time must be even longer. As there is no way to remotely power on (the device itself being the means of wireless communication), the Photon must be constantly powered for the duration between initially pumping down to vacuum and the final recording of the GoPro. Given the time to pump down, any delay between achieving vacuum and attempting to fire, and the time it may take to successfully fire, the Photon must be powered on overnight. This consumption was initially attributed a window of 48 hours in case there were any unanticipated delays with attempting to fire. Prior to pumping down, a charging cable will be fed through the window of the chamber to ensure that both batteries are fully charged.

The following table summarizes the power consumption specifications for both devices. Here, the consumption information is displayed for the GoPro in Wifi mode while engaging with a smartphone (it would be off otherwise) and the Photon in standby mode (as the period in which it would be running code, 30 for Mylar scrolling, is very minimal in comparison):

As a safety factor to ensure that all devices would be powered on to capture the footage when the moment comes, this total energy consumption was doubled to 61.848 Wh when sizing for a battery. This would allow for, as an example, 12 hours of GoPro power (for an entire day of engaging with the thruster), and 72 hours of Photon power (enabling wireless communication for up to a week under vacuum). Of course, the actual proportion of battery capacity for each device will depend on their actual usage. Lastly, to ensure longevity of battery life, Lithium ion batteries should be discharged to no more than 25% of their capacity or 75% Depth of Discharge (DOD). Taking this into account, The battery selected for this application should have a capacity of at least 82.464 Wh. As USB power is rated at 5V, this would equate to 16492.8 mAh.

Beyond just meeting the necessary capacity while maintaining reasonable dimen-

Table 3.2: USB Battery Bank Power Consumption Analysis

Parameter	Symbol	Measurements
GoPro Hero 5 Session		
Voltage	V_G	3.8 V
Discharge Current	I_G	750 mAh
Power Consumption	P_G	2.85 W
Duration	t_G	6 hrs
GoPro Energy Consumption	E_G	17.1 Wh
Particle Photon		
Voltage	V_P	4.8 V
Current	I_P	80 mAh
Power Consumption	P_P	0.384 W
Duration	t_P	36 hrs
Photon Energy Consumption	E_P	13.824 Wh
Total Energy Consumption	E_T	30.924 Wh

sions, one key requirement for the video diagnostic system is that the li-ion battery circuitry allows for pass-through charging. The vast majority of USB battery packs cannot power devices while being charged themselves. While this fact in and of itself is not necessarily a problem since charging will halt before the tank is pumped down to vacuum, it usually requires a button on the battery to be pressed to enable discharging. This may be especially problematic, as the system would be mounted in place a few days prior to pumping down, in order for researchers to coat all surfaces of the tank in foil. Once the foil is in place, one can no longer enter the tank to press a button or turn a switch. Attempting to reach a button from the nearest window would also be extremely challenging. Battery packs with pass-through charging allow the devices to be powered regardless of whether the battery is being charged, and without the use of any buttons. Therefore, the GoPro and Photon will be powered by the battery pack while it is charging, and a researcher will simply pull out the charger from the window without affecting anything.

Looking at battery banks that meet these specifications, the Zendure A5 16,750 mAh portable battery pack was selected, with 2 USB ports that allow for direct charging of both devices without the use of a splitter. With pass-through charging and a capacity well suited to the energy consumption, the Zendure battery is an excellent fit for the system.

12V Battery - Sizing & Selection

As the mylar scrolling mechanism will run continuously (as opposed to the intermittent solenoid actuators), the 12V battery was sized exclusively from the power consumption of the motor. Since the Mylar scrolling would only be activated for a successful firing of the thruster (and recording would occur for only a portion of a run), the consumption time this battery needs to be sized for is significantly shorter. The calculations were initially based on recording for a standard firing time of approximately 30 minutes:

Table 3.3: 12V Battery Sizing

Parameter	Symbol	Measurements
Max Current	I	1.2 A
Motor Voltage	V	12 V
Power	P	14.4 W
Recording Duration	t	30 min
Energy	E	7.2 Wh
Battery Capacity	C	0.6 Ah

The above table summarizes the calculations for the necessary battery capacity for 30 minutes of active recording. To allow for multiple runs, this capacity was doubled to 1.2 Ah to allow for up to an hour of active recording. Searching for batteries of this capacity, it proved difficult to find an appropriately sized 12V lithium ion battery. It may be possible to string multiple smaller batteries together, but doing so may lead to additional complications with battery management. As a result, a Sealed Lead Acid (SLA) battery was selected for this application instead. To preserve battery life, the SLA battery was sized to be discharged to only 60% DOD. Scaling up for this DOD, a 12V 2Ah SLA battery from Power Sonic was selected for the system.

Charging Circuit

For convenience on the user end, a circuit was designed that would enable both batteries to be charged from a single charger. If the BNC feed thru on the tank wall were to be used instead of a cable through an open window, a single charger would be a requirement. Using this pre-existing feed thru would even allow the batteries to remain charged while under vacuum. This may be especially useful if the tank is kept at vacuum for longer periods of time, for example if a change in propellant allowed

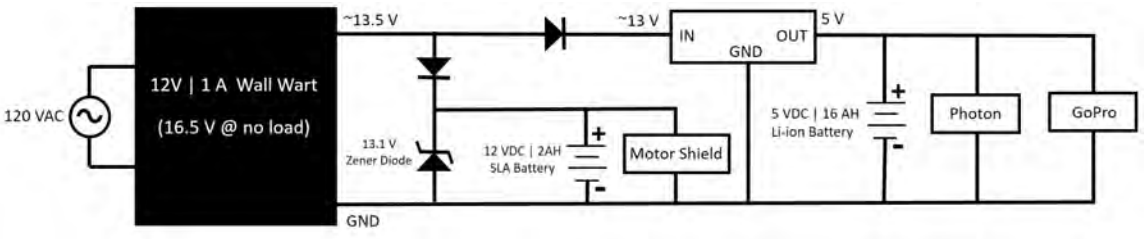

Figure 3.13: Charging Circuit.

for multiple days of testing without the need for significant clean up.

The circuit diagram in Figure 3.13 illustrates both the wiring schematic for charging both the batteries, as well as their respective loads. By using diodes in each line, one can charge two batteries in parallel without the risk of one battery charging the other once the charger is unplugged. As the SLA battery has a significantly smaller capacity than the li-ion battery pack (24Wh vs. 83.75Wh), not isolating the batteries may lead to the SLA draining before the camera even starts recording.

To charge the batteries, a 12V — 1A wall wart was used. Measured at 16.5V with no load, this particular adapter is still remains above 13V when charging the batteries, rising up to approximately 13.8V once the batteries are fully charged. Upon reaching the camera housing, the positive lead will split to charge the two batteries in parallel. One line goes directly to the 12V SLA battery, which in turn is wired to the DC input of the Adafruit Motor Shield via a barrel jack adapter. The other line, in order to power the USB battery pack, is stepped down via a 12V to 5V DC/DC converter with a miro-usb adapter, which plugs directly into the battery pack. This battery in turn recharges the GoPro and provides constant power to the Photon via the two USB ports.

To regulate the charging voltage for the SLA battery, which features no internal circuitry of its own, a 13.1V Zener diode is used in parallel, ensuring that the battery will not be damaged. If the system will be left unplugged for significantly longer than designed for, it is recommended that a low voltage disconnect relay be added in between the SLA battery and the Adafruit motor shield. Cutting off the battery at approximately 11V would result in a significantly increased lifespan.

3.1.7 Cooling

To keep all heat generating components at safe operating temperatures, an aluminum cooling block was used to transfer heat out of the housing to a water pipe in the back of the tank. The GoPro, Photon and motor shield, and the two batteries are all connected to this block. To facilitate implementation, the cooling block would be directly mounted to the back wall, from which heat would transfer via conduction through the wall to the water pipe on the other side.

Modeling the block as one directional heat flow to the back wall and assuming steady state heat conduction, Fourier's law was used to estimate the minimum cross sectional area of the block

$$q = -kA\frac{dT}{dX}, \tag{3.1.2}$$

where q is the heat transfer in watts, k is the thermal conductivity of the material in W/mK, A is the area of the cooling block (m^2), and dT/dX represents the temperature gradient in K/m. Solving for A and breaking down the temperature gradient into its input parameters

$$A = \frac{-qL}{k(T_{max} - T_{water})}, \tag{3.1.3}$$

where T_{max} represents the maximum operating temperature of the electronic components (set to 25°C to be safely under the GoPro limit), and T_{water} is set to be at 15°C. L, the length of the block is set at 20.32cm. Lastly, a value for q is estimated with a large margin of error by assuming that half of the power consumption goes directly to heat (8.817 W).

This heat flux analysis results in a recommended cross sectional area of approximately 1.157 in^2. Using 3" as the width of the block due to spacing requirements (see Section 3.2.1) results in a thickness of 0.386." To save machining time, and for an extra margin of error, this thickness was rounded up to the next size that was commercially available: 0.5".

3.2 System Integration

The following section describes how the various components of the system were integrated into a cohesive system. Modeling each of the designs in PTC CREO Parametric 3.0, the various components were edited an assembled into an optimal configuration that prioritized compactness while maintaining manufacturability and ease of system maintenance.

3.2.1 Housing

With all parts assembled, it as determined that the system can fit primarily within a box constructed out of 8" x 8" sheets of aluminum. Aluminum was selected as it provides adequate structural integrity for the components within, exceeds the temperature requirements of the environment behind the heat shield, and is relatively easy to machine compared to metals such as steel. The 8" x 8" sheets were the minimum commercially available size that would encompass all components in the assembly. Keeping the walls at the stock dimensions whenever possible would also decrease the chances of misalignment during assembly, and milling them down further would add significant machining time without a significant increase in overall compactness.

1/4" thickness was selected for the walls as it wide enough for holes to be tapped and threaded for bolts during assembly. #6-32 steel socket cap screws were then used, providing more than enough strength for the given loads. These screws were used throughout the system to avoid the need for multiple allen wrenches when a researcher would enter the tank. Ultimately, a small portion of #8-32 and #4-40 screws were also needed within the box due to pre-existing mounting holes for the solenoid actuators and the microcontroller.

Figure 3.14 shows the outer dimensions of the box. While 8" x 8" sheets were sufficient to house all components, the side walls extend to 9.25", an inch past the front wall, for mounting both the shutter system and outer shafts of the film scrolling mechanism (see 3.15). The top and bottom walls were mounted in between the side walls to maximize space within, increasing the width to 8.5" while retaining the box height at 8". To allow for ease of maintenance, a 7.5" x 8" portion of the right wall of the box is designed to be removable, with no internal components attached to it. Subsequent images of the system will not include this wall in order to display the parts within.

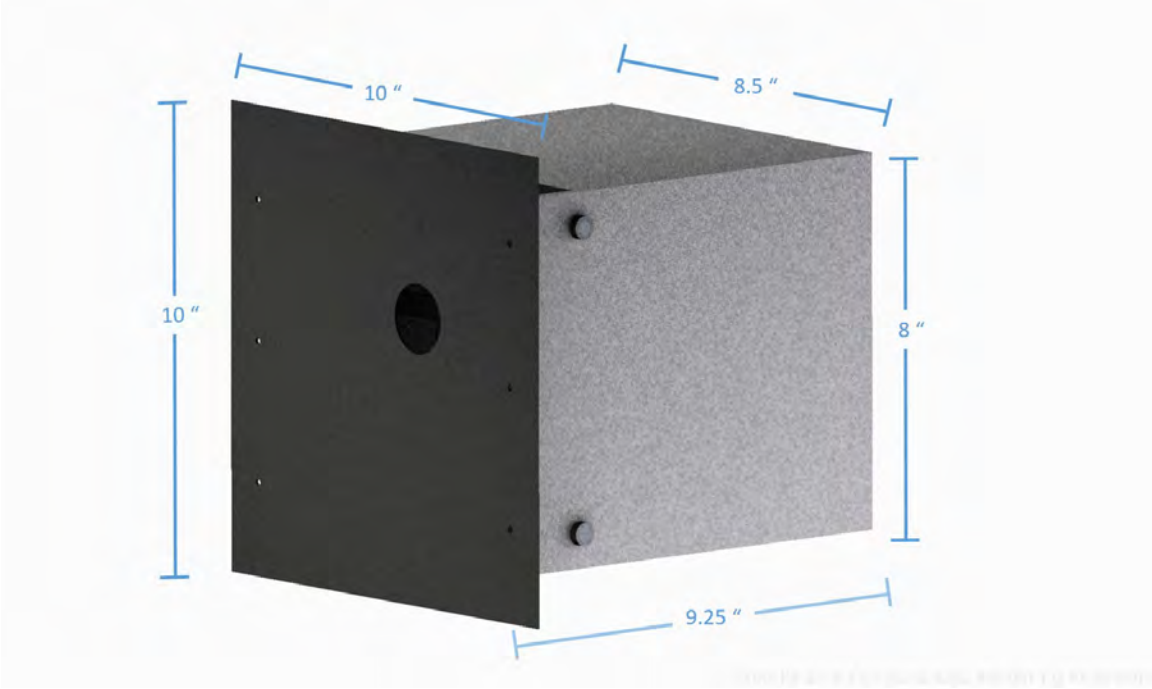

Figure 3.14: Outer Dimensions of the LiLFA Video Diagnostic System. [CREO Rendering]

Lastly, the 10" x 10" heat shield is mounted 1" in front of the box via six #6-32 screws.

3.2.2 Internal Assembly

Figure 3.16 provides a front on view of the system without the heat shield. The solenoid, mounted to the front wall, rotates the shutter piece in front of a 1" window for the camera inside. This hole is fitted with an 1/8" thick glass disc for an additional layer of protection. The Mylar film will scroll from the outer bottom shaft to the outer top shaft, positioned so that the film will run in between the shutter and the glass.

Figure 3.17 provides a front on view of the system behind the front wall. It displays the internal top and bottom dowels, the square face DC gearmotor that rotates the top shaft, and the sprockets for the chain drive that spin the bottom shaft. The GoPro, mounted to the cooling block, is positioned directly behind the filter mechanism which slides the glass along the block to cover the lens. Also pictured is the USB battery pack, positioned directly below the cooling block for heat transfer, and supported by a 1/4" thick aluminum battery tray that can be adjusted for a secure fit.

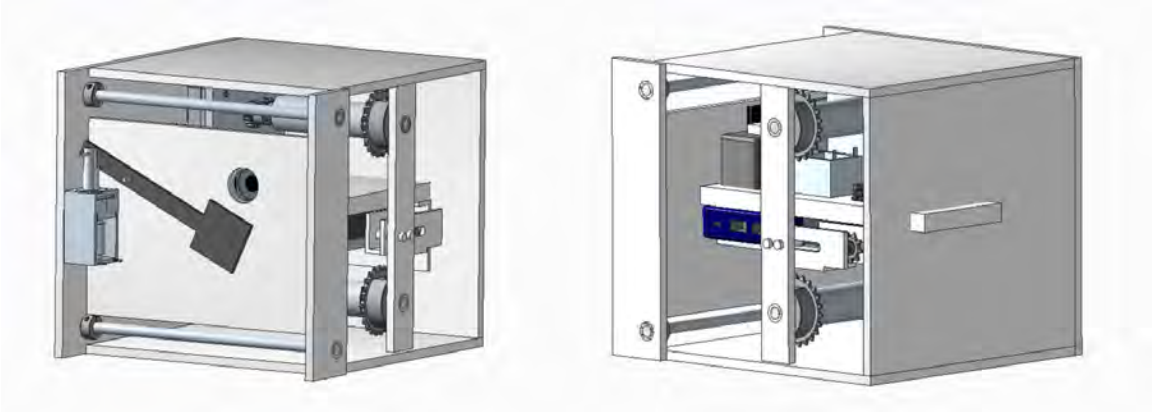

Figure 3.15: 3D view of housing with heat shield and side wall removed. [CREO Rendering]

The remaining internal components are shown through a profile view in Figure 3.18. The solenoid actuator for the remote power on mechanism is positioned directly behind the GoPro, and mounted to the cooling block through an 1/8" L bracket. On the back end of the cooling block is the microcontroller, mounted via standoffs so as to not short the pins on the bottom. Pictured below the block is the full battery tray, which supports the USB battery pack to the left and the 12V SLA battery on the right. Connected to the cooling block via two #6-32 threaded rods, the tray is secured in place via lock nuts to ensure that the top surfaces of the batteries have firm contact with the block for heat transfer. Lastly, to enable the side wall to be removable for ease of maintenance, it should be noted that an additional bar of aluminum was used within the box to support the top and bottom shafts of the chain drive, as well as the tensioner.

Lastly, Figure 3.19 provides an additional top down view of the cooling block, to better demonstrate the layout of the components. The filter is positioned in the small gap between the camera and the front wall, with enough space so that it will not be rubbing against either surface. The GoPro itself is secured onto the cooling block through a clamp constructed from an aluminum stand off and #6-32threaded rod, as well as a 0.2" deep groove cut into the block to prevent the camera from shifting due to the push from the solenoid. A small channel was also cut to guide the 1/8" aluminum piece at the end of the solenoid as it slides toward the button on the back of the camera. Lastly, to ensure that the microcontroller is kept at a safe operating temperature while under vacuum, copper strips were glued onto each of the chips on the Photon, motor shield, and shield adapter with epoxy rated for high temperature environments. These strips were then screwed onto the cooling block to

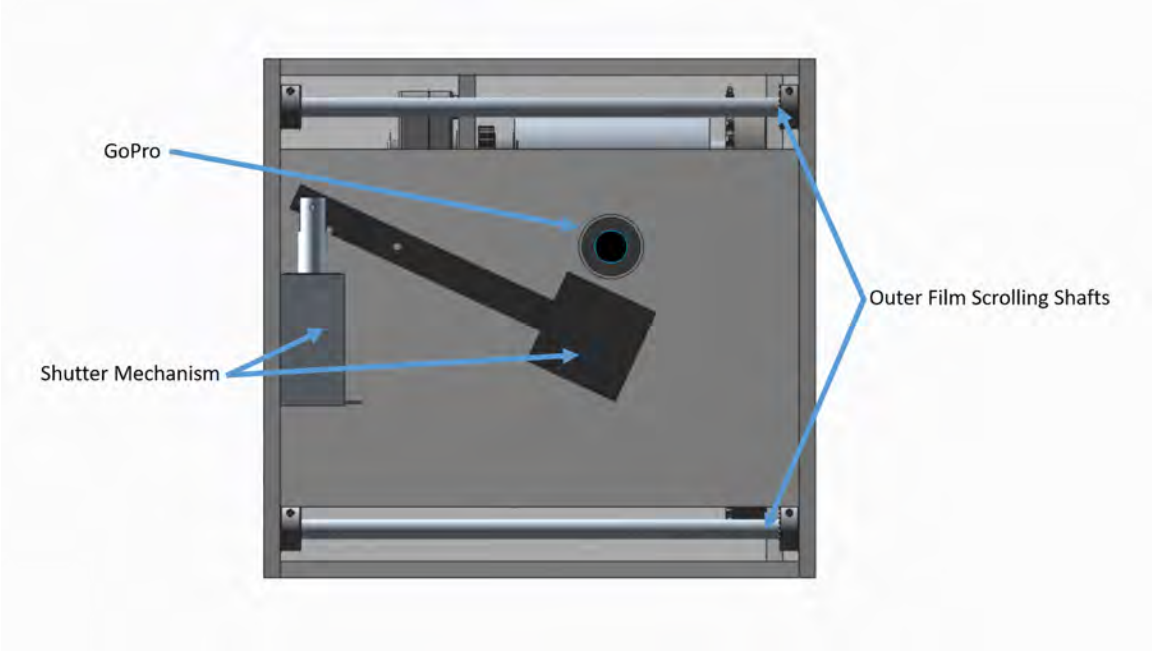

Figure 3.16: Front view with heat shield removed. [CREO Rendering]

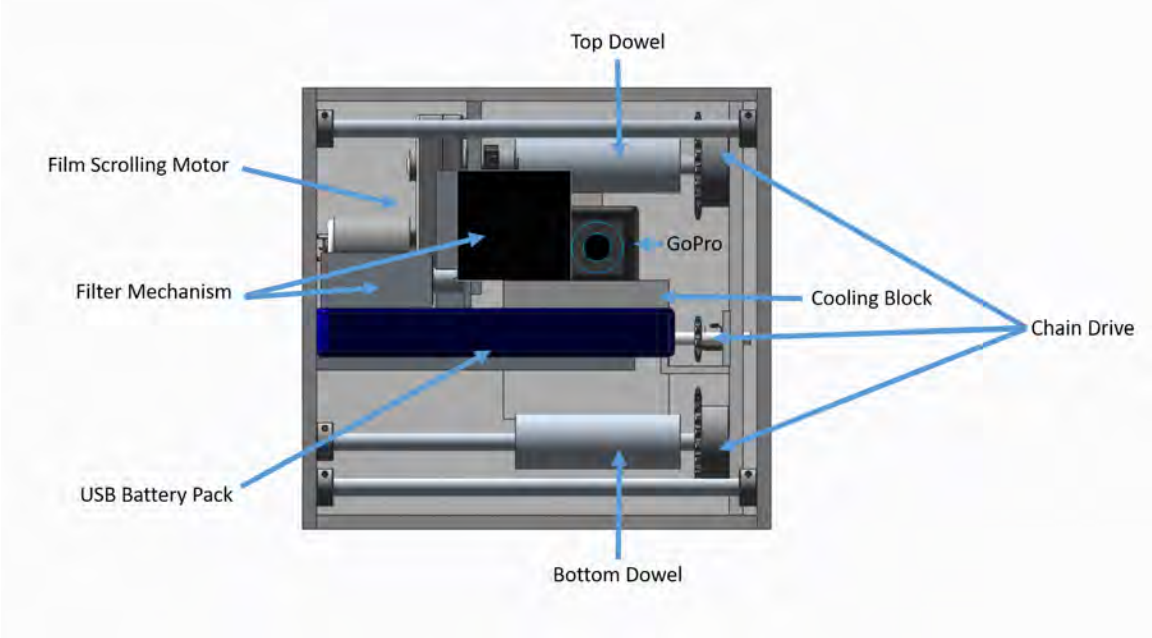

Figure 3.17: Head on view with heat shield and front wall removed. [CREO Rendering]

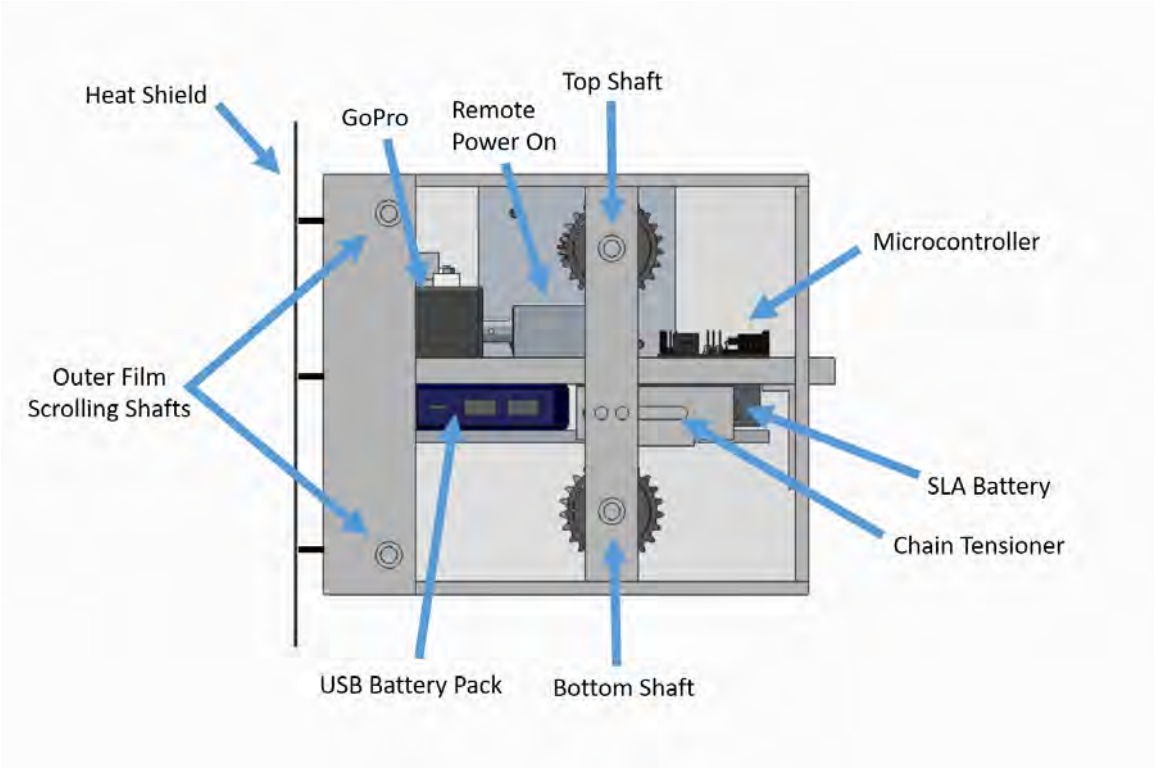

Figure 3.18: Profile view with side wall removed. [CREO Rendering]

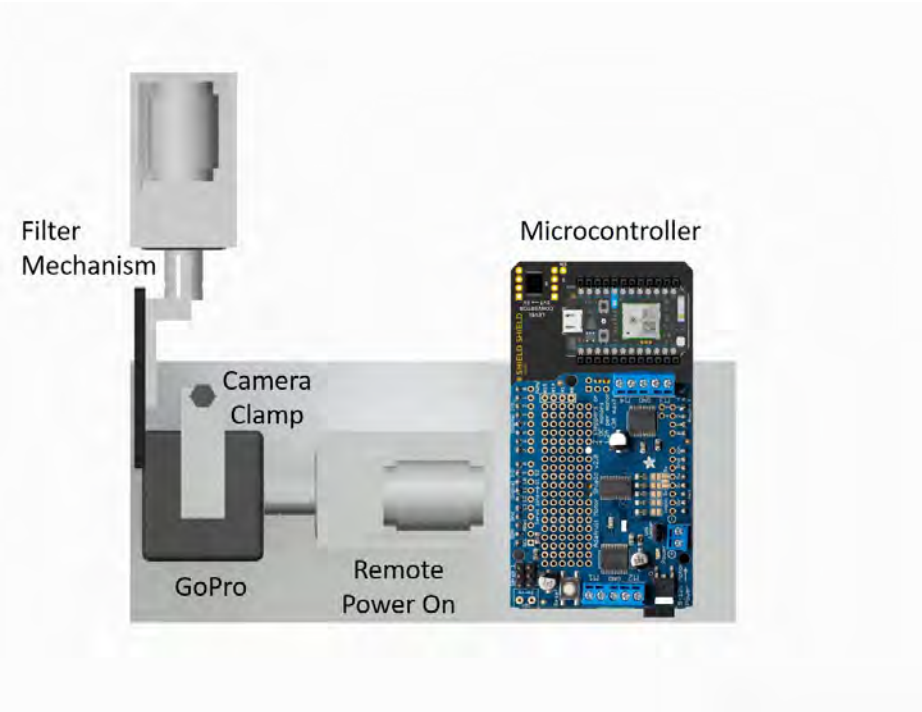

Figure 3.19: Cooling Block Setup.

provide a direct channel for heat transfer off of all heat generating elements on the circuit boards.

3.2.3 Installation

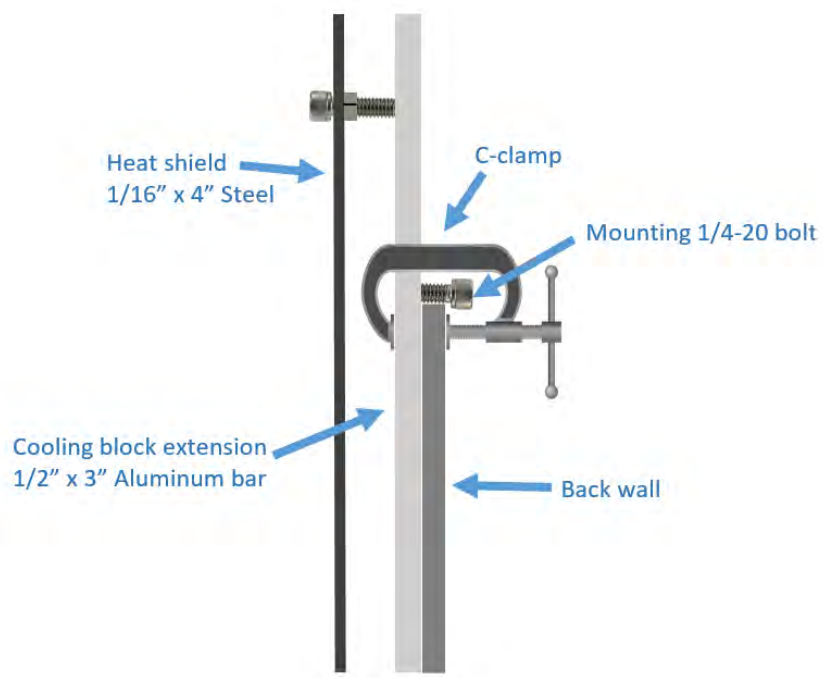

Figure 3.20: Schematic of mounting structure]

To mount the video diagnostic system against the back wall of the vacuum, a 2 1/2 foot long 3" x 1/2" aluminum bar is used as an extension of the cooling block to reach over the back wall. For this purpose, the cooling block within the box protrudes 1/2" outwards through a slit, to allow for connection to the mounting structure via 1" #1/4"-20 socket cap screws. To prevent any torque on this juncture, an additional aluminum block was installed at the top of the box as a second point of contact with the mounting bar. The mounting bar would be secured onto the back wall via two more #1/4"-20 that serve as hooks, as well as a C-clamp to ensure firm contact with the wall for heat transfer to the water pipe on the other side. Figure 3.20 provides a schematic of the wall mounting configuration.

Chapter 4

Testing and Results

4.1 Completed Video Diagnostic System

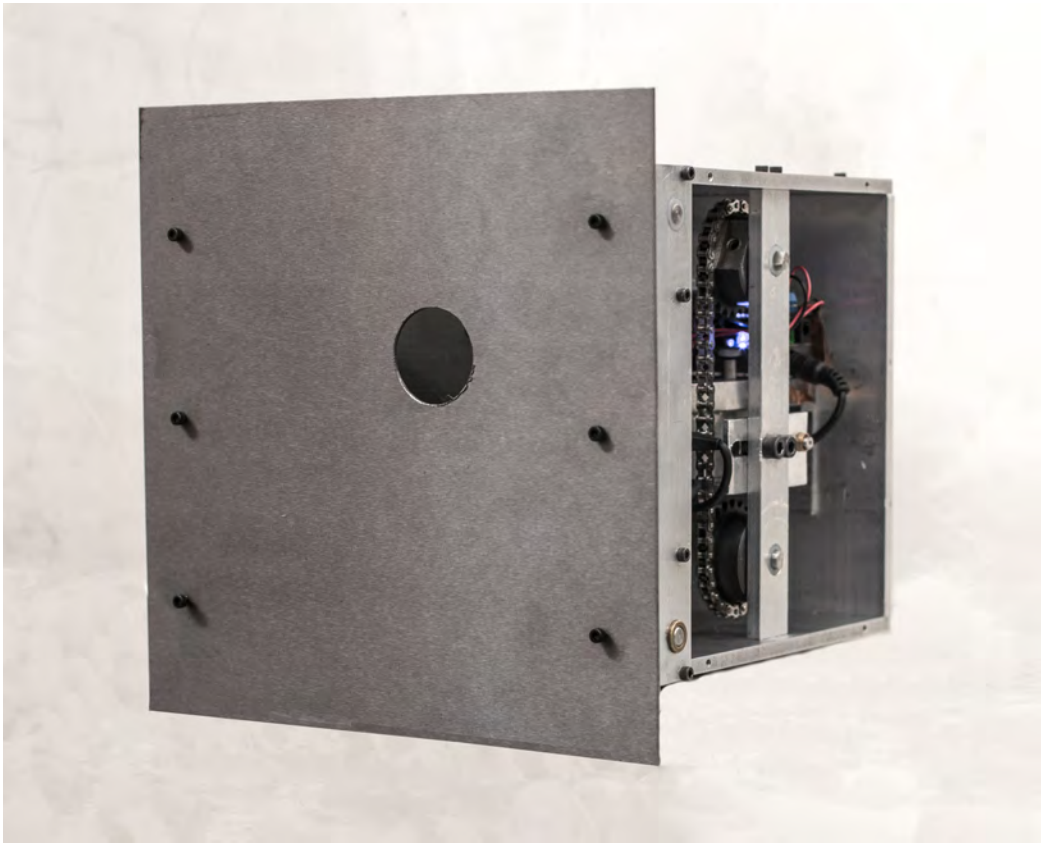

Figure 4.1: Full system with wall removed for internal display.

Figures 4.1, 4.2, and 4.3 show the fully assembled system. All components were manually machined on the mill and lathe in the EPPDyL, with the exception of the steel heat shield for which a CNC milling machine was used to make the 1.5" diameter hole. Most of the wiring is run through the space behind the motor and batteries to prevent interference with the film scrolling mechanism. The top down perspective provided in Figure 4.4 provides a better view of the electronics.

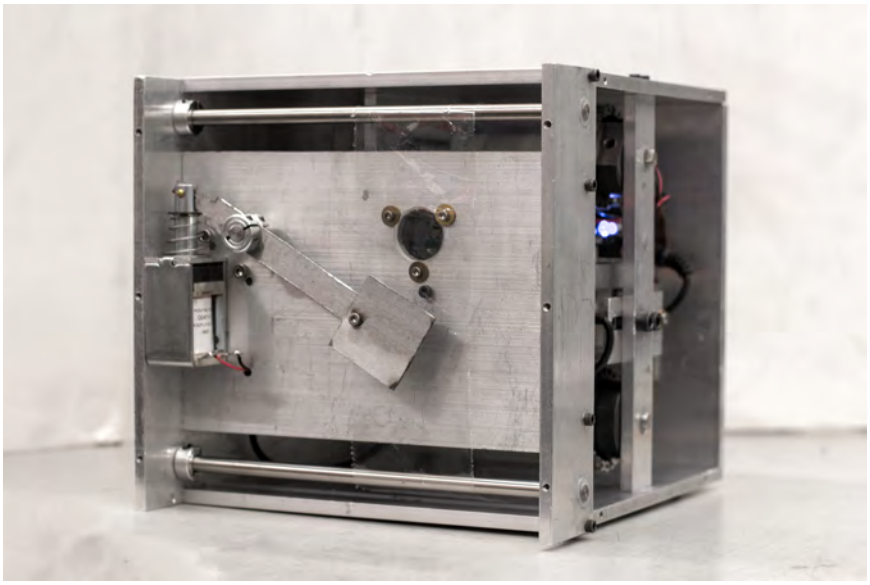

Figure 4.2: Assembled system with heat shield removed.

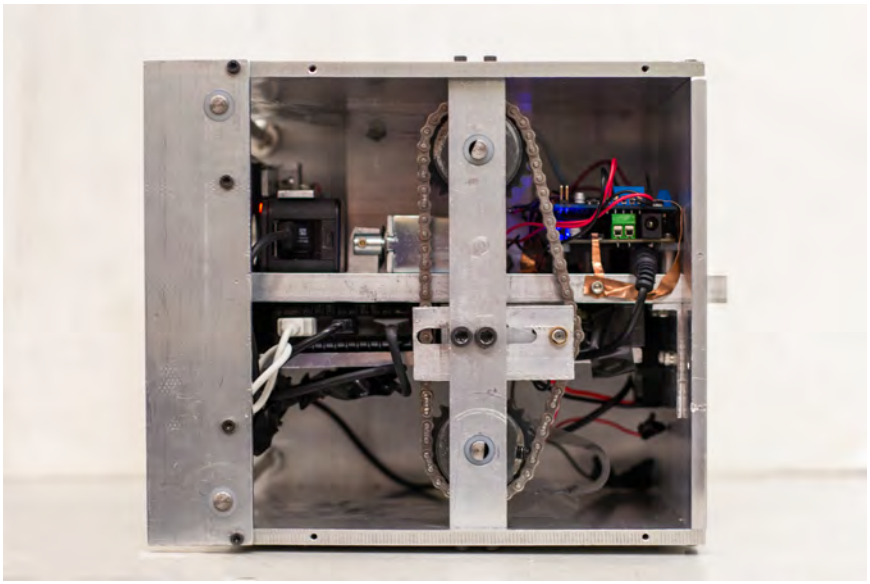

Figure 4.3: Profile view of assembled system.

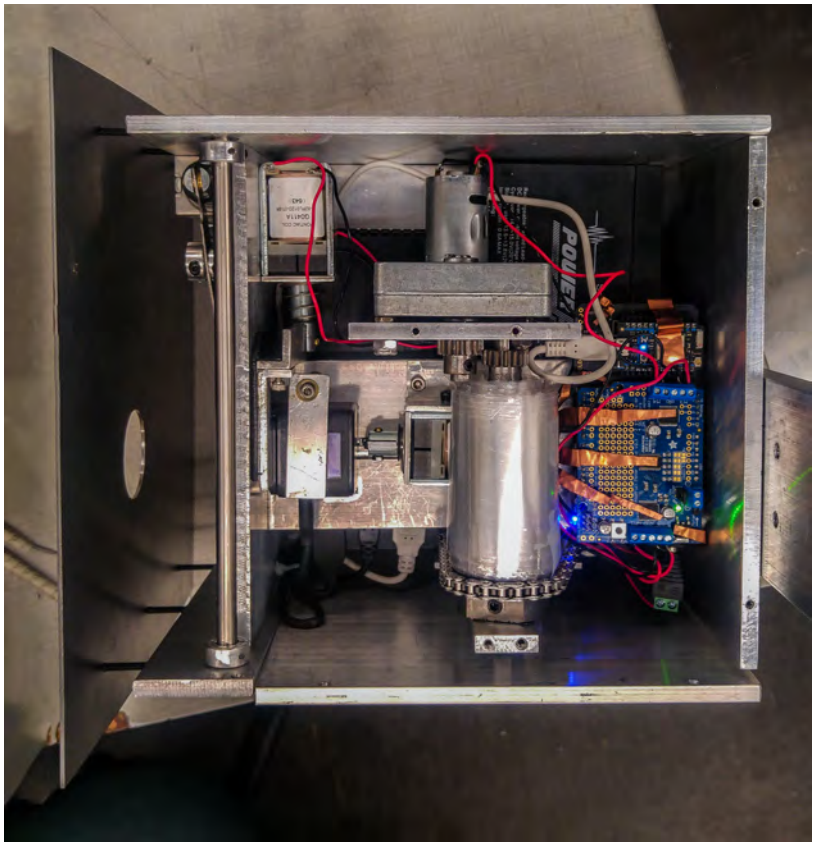

Figure 4.4: Ceiling removed for top down view of internal layout.

4.2 Testing

Several tests were run prior to and after project implementation to ensure successful operation of the system. These ranged from testing basic functionality of electronics and controls, to ensuring that all components of the system could successfully operate in vacuum and run for the necessary duration.

4.2.1 Vacuum Tests

Camera Vacuum Test

Prior to any machining, the camera itself was tested in the vacuum chamber. There have been reports of GoPro models being used successfully in vacuum environments,

but they will automatically power off to prevent overheating if there is no medium for heat to transfer out through.

The camera was placed behind a side window of the tank, making contact with the steel surface. Monitored through a live feed via the GoPro app, the camera successfully recorded for a full 30 minutes under vacuum before venting the chamber back up to atmospheric pressure. Communication was sustained throughout, and there were no signs of damage such overheating or outgassing when the camera was retrieved.

Battery Vacuum Test

Once it was confirmed that the GoPro could operate successfully under vacuum, the USB battery pack was similarly tested while using the discharged camera as a load. Both the battery and the GoPro were placed on an aluminum block on the floor of the vacuum chamber, which was pumped down for several hours. Upon retrieval, there were no signs of damage on either device, and the battery continued to function normally during future uses in both vacuum and atmospheric pressure.

Full System Test

With the system fully assembled, the Photon and motor shield could now be tested in configuration with the 12V SLA battery as all chips were connected to the cooling block via copper strips. A program was loaded onto the controller to continuously power the motor at a high film scrolling speed (30rpm), and the environment was pumped down to vacuum. After 30 minutes, the chamber was vented back up to atmospheric pressure. The program was still running and there were no signs of overheating from any components in the system. Later, the system was installed in the back of the steel tank (see Figure 4.5), where it will remain under vacuum for several months.

4.2.2 Communication and Control Tests

Prior to machining the camera housing, the Photon and motor shield configuration was tested to ensure that the motor and solenoid actuators could be controlled as in-

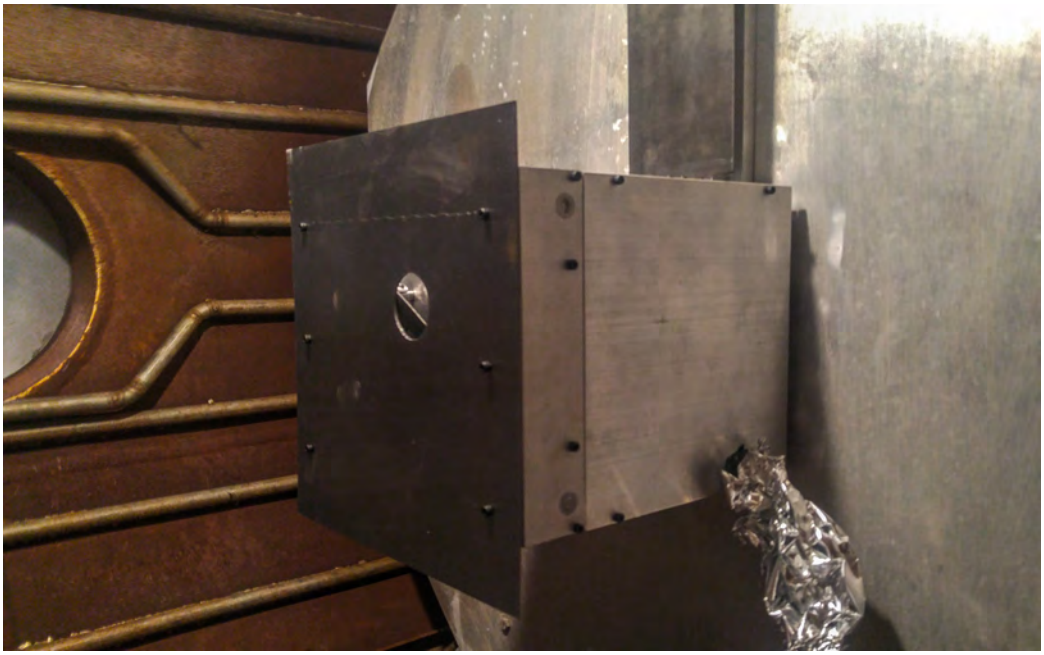

Figure 4.5: System mounted against back wall of steel tank.

tended. All loads were wired to the four ports on the motor shield, and the lithium ion and SLA batteries were connected to the Photon and motor shield respectively. Code was sent to the Photon to run them all on a loop, all four components successfully operated for the duration of the test. See Appendix A for testing code.

The setup was also used to determine ideal parameters for future scripts, such as the PWM value corresponding to the desired rpm of the motor (100 - 150 for normal operation), as well as the duration of the pulse for the solenoid actuators (250 milliseconds). This script was also used for the vacuum test once the system was fully assembled.

Wifi Signal Strength

The signal strength was also tested during final vacuum tests upon installation. As the GoPro contains its own Wi-Fi transmitter for the camera's network, communication is dependent on proximity to the camera. Through both initial testing and installation, the Wi-Fi connection was established when standing outside of the steel tank.

The microcontroller, on the other hand, depends on communication with the nearest router for its connection to the cloud. Although the Photon was capable of connecting to the Wi-Fi network while enclosed in the aluminum box, the signal was not strong

Figure 4.6: Particle rubber duck antenna and cable.

enough to reach it when the box was placed in the back of the steel tank. To boost the signal strength, a rubber duck antenna (pictured in Figure 4.6) was mounted on top of the box where it is protected by the mounting bar heat shield. An RP-SMA to u.FL interface cable was used for direct connection to the Photon. By installing the antenna in this position, there would be no signal obstructions between the microcontroller and the tank window. Programming the Photon to look to the external antenna for Internet connection, the constant communication was successfully established upon re-installation.

GoPro Interface

Figure 4.7: View of thruster from GoPro mobile app.

During development of the video diagnostic system, the GoPro was configured using the accompanying GoPro App, available for both iPhone and Android. Figure 4.7 is a screenshot of the streaming interface, and provides the view of the thruster that will be captured when the system is mounted in the back of the steel tank.

For use by researchers however, it is more convenient to control the GoPro from

a laptop. This prevents the need for additional devices such as a smartphone or tablet. In doing so, footage can also be directly downloaded to the device on which it will be analyzed. While the camera provides the network name and password on its LCD display, the 4^{th} and 5^{th} generation of GoPros require an extra pairing step that prevents a quick connection from any laptop. This extra security feature was addressed by the Camera Suite software, an application compatible with PC and Mac that enables the user to pair with the camera, and control all settings and recording functions. Figure 4.8 provides a screenshot of the software with a live stream of the thruster. The Camera Suite application also enables the user to sort through and download files from the camera's Micro SD card for reviewing footage in higher definition, and later syncing it with other data collected while firing.

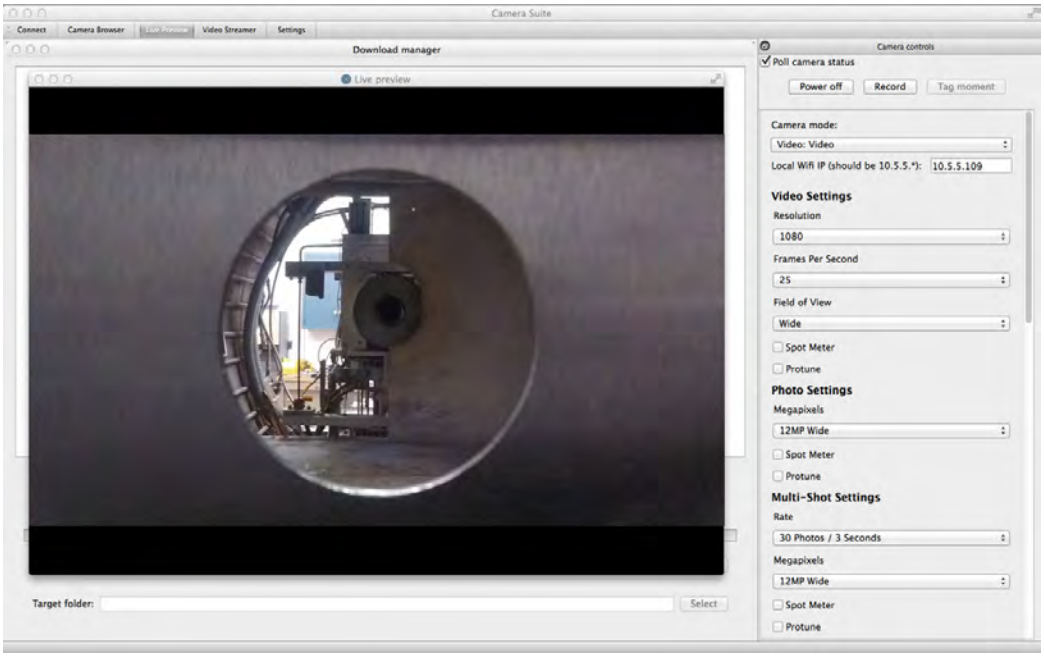

Figure 4.8: Camera Suite Mac user interface.

4.2.3 Battery Tests

While the li-ion battery pack was sized to power the photon for several days beyond what is required for normal thruster firing procedures, it was critical that the SLA battery be tested as it is sized for operating for only an hour. The battery was fully charged and powered the motor shield as the Photon ran the testing script.

For the first 48 minutes, all components operated normally. Subsequently, the shutter

would only close intermittently, at first during every other iteration of the loop, and then every third and fourth iteration. By 1 hr 50 min, the shutter failed to close, while the motor continued to run at a slower rate. At this point, the battery was disconnected as it was already discharged significantly past the recommended level of 60% DOD.

The system therefore operated perfectly for only 80% of the time the battery was sized for, but this is still far beyond what is expected for normal use. The longest operation of the LiLFA was on the order of 30 minutes, and researchers intend to obtain footage for no more than 10 to 15 minutes. As a result, doubling the required capacity when sizing the battery will allow for successful system operation, even as the battery capacity declines over time.

4.2.4 Obtaining Thruster Footage

Figure 4.9: Footage from thruster firing.

While the tests prove that the video diagnostic system can successfully operate under vacuum for longer than the required duration, it has yet to obtain head on footage from a thruster. While the project was being implemented the propellant was switched to argon for testing of a new thruster. Furthermore, there were only two occasions on which this thruster was actually fired thus far, and the system was not ready to be mounted inside the vacuum chamber at the time.

Instead, footage was obtained from a mirror pointed at the thruster during these runs. Although far from ideal, it provided sufficient visual as the mirror would no longer be coated in lithium under the new propellant. From the footage obtained, an

optimal shade of welding glass (Shade #6) was also selected. Figure 4.9 provides a sample frame of the footage obtained during this test.

4.3 Conclusions

Although several design alternatives could be pursued for the given application, the system developed is well suited for the extreme environment in which footage is to be obtained, and has proven successful under the testing conducted. Manufacturability and ease of maintenance was considered throughout all aspects of the design, and the system provides a decent amount of flexibility should the camera be used under parameters different from what it was originally intended for. The motor selected will enable future researchers to adjust scrolling speeds according to the mass deposition rate of the propellant, and the sizing of the batteries will enable the system to last for significantly longer should a change in propellant allow researchers to fire on multiple days without venting up the tank for cleaning. Lastly, should the batteries ever need replacing, the adjustable height of the battery tray will allow for different sized batteries to be used, ensuring system sustainability as this form of electric propulsion continues to be studied and developed.

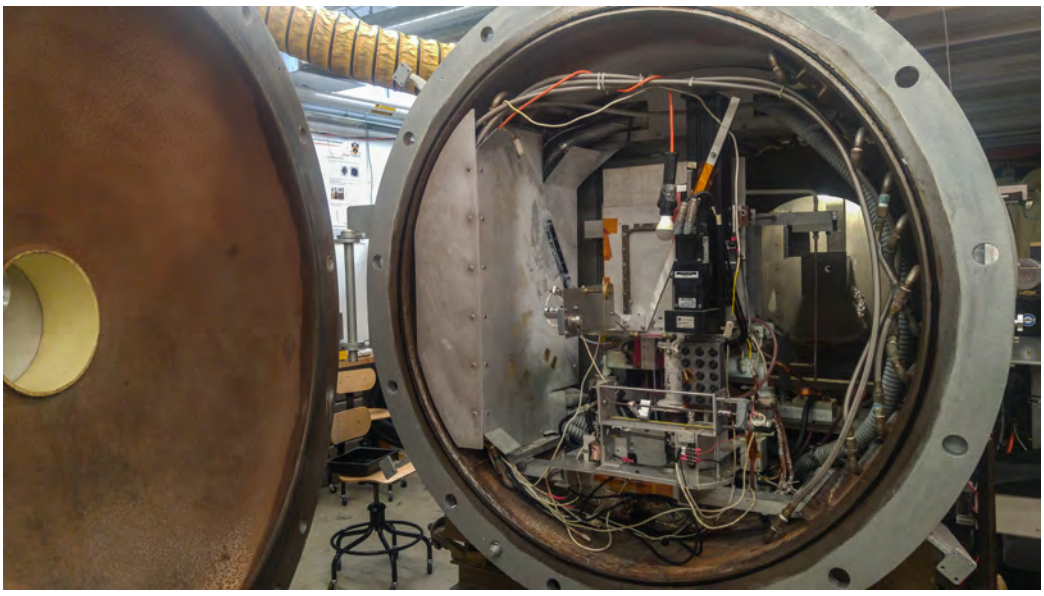

Figure 4.10: Full view of tank with video diagnostic system installed.

Bibliography

[1] Max Born and Emil Wolf. *Principles of Optics, Electromagnetic Theory of Propagation, Interference, and Diffraction of Light*. Pergamon Press, 1964.

[2] Will Coogan and Michael Helper. Lithium lorentz force accelerator (lilfa). poster, 2015.

[3] Will Coogan, Michael Hepler, and Edgar Y. Choueiri. Dynamic resistance probe for the measurement of the mass deposition rate from a condensible propellant thruster. In *34th International Electric Propulsion Conference*, 2015. IEPC-2015-199.

[4] Robert G. Jahn. *Physics of Electric Propulsion*. Dover Publications, 1968.

[5] Thomas Kramer. 3-d characterization of the plume of a lithium lorentz force accelerator (lilfa). bscthesis, 2003.

[6] Electric Propulsion and Plasma Dynamics Laboratory. What's electric propulsion: Electromagnetic. [Online; accessed 1-May-2017].

[7] SpaceX. Spacex interplanetary transport system, 2016.

[8] TLX Technologies. Latching solenoid theory. [Online; accessed 12-Jan-2017].

[9] Wikipedia. Worm drive — Wikipedia, the free encyclopedia, 2011. [Online; accessed 12-Jan-2017].

Appendix A

Sample Testing Code

```
#include <application.h>
#include <Adafruit-MotorShield-V2.h>
#include <Adafruit_PWMServoDriver.h>

/*
 Visit the following url for help on connecting the motor shield
 to the spark core:
 https://community.spark.io/t/adafruit-motor-shield-v2-progress/5218
*/

// defining which component is connected to which port
Adafruit_DCMotor *buttonPusher = AFMS.getMotor(3);
Adafruit_DCMotor *filter = AFMS.getMotor(1);
Adafruit_DCMotor *shutter = AFMS.getMotor(2);
Adafruit_DCMotor *mylarMotor = AFMS.getMotor(4);

void setup() {
  Serial.begin(9600);           // set up Serial library at 9600 bps
  Serial.println("Adafruit Motorshield v2.3 - Video Diagnostic System
   Test");

  // initialize digital pin LED_BUILTIN as an output.

```

```
  AFMS.begin();  // create with the default frequency 1.6KHz
  // turn on motor
  mylarMotor->run(RELEASE);
}

void loop() {

uint8_t i;
mylarMotor->run(FORWARD);

for (i=0; i<100; i++) {

  if((i % 2) == 0) {

    //run motor forward for 1 minute
    mylarMotor->run(FORWARD);
    mylarMotor->setSpeed(200);
    delay(60000);
    mylarMotor->setSpeed(0);
    delay(1000);

    //turn on filter
    filter->run(Forward);
    filter->setSpeed(255);
    delay(250);
    filter->setSpeed(0);

    //open shutter
    shutter->run(FORWARD);
    shutter->setSpeed(255);
    delay(250);
    shutter->setSpeed(0);

  //press GoPro "ON" button
    buttonPusher->run(FORWARD);
    buttonPusher->setSpeed(255);
```

```
59      delay(250);
60      buttonPusher->setSpeed(0);
61
62      }
63
64    else {
65
66      //retract button pusher
67      buttonPusher->run(BACKWARD);
68      buttonPusher->setSpeed(255);
69      delay(250);
70      buttonPusher->setSpeed(0);
71
72      //run motor backward for 1 min
73      mylarMotor->run(BACKWARD);
74      mylarMotor->setSpeed(200);
75      delay(50000);
76      mylarMotor->setSpeed(0);
77      delay(1000);
78
79      //close shutter
80      shutter->run(BACKWARD);
81      shutter->setSpeed(255);
82      delay(250);
83      shutter->setSpeed(0);
84
85      //turn off filter
86      filter->run(FORWARD);
87      filter->setSpeed(255);
88      delay(250);
89      filter->setSpeed(0);
90
91       }
92      }
93 }
```